

Electronic Supporting Information

Cucurbit[7]uril Complexations of Good's Buffers

Allison J. Selinger and Donal H. Macartney

Department of Chemistry, Queen's University, Kingston, ON K7L 3N6, Canada
dhm@queensu.ca

Table of Contents	Page
Figure S1. Limiting CB[7] complexation-induced chemical shift changes ($\Delta\delta_{lim}$, ppm) for the proton resonances of the cyclohexylamino buffers in D ₂ O (pD = 4.75, 0.050 mol dm ⁻³ NaOAc-d ₃ /0.025 mol dm ⁻³ DCI).	4
Figure S2. Plot of complexation-induced shift in the proton resonance H _{3a,5a} for CHES (0.965 x 10 ⁻³ mol dm ⁻³) as a function of [CB[7]] in D ₂ O (pD = 4.75, 0.050 mol dm ⁻³ NaOAc-d ₃ /0.025 mol dm ⁻³ DCI). The solid curve is a fit to a 1:1 binding model using $K_{CB[7]} = 3.60 \times 10^7$ dm ³ mol ⁻¹ and $\Delta\delta_{lim} = -0.704$ ppm.	4
Figure S3. ¹ H NMR (300 MHz) titration of CAPS (1.02 x 10 ⁻³ mol dm ⁻³) with (a) 0.00, (b) 0.18, (c) 0.42, (d) 0.60, (e) 0.82, (f) 0.92, (g) 0.98, (h) 1.14, (i) 2.05, and (j) 4.52 equivalents of CB[7] in D ₂ O (pD = 4.75, 0.050 mol dm ⁻³ NaOAc-d ₃ (*))/0.025 mol dm ⁻³ DCI).	5
Figure S4. Plot of complexation-induced shift in the proton resonance H _γ for CAPS (0.990 x 10 ⁻³ mol dm ⁻³) as a function of [CB[7]] in D ₂ O (pD = 4.75, 0.050 mol dm ⁻³ NaOAc-d ₃ /0.025 mol dm ⁻³ DCI). The solid curve is a fit to a 1:1 binding model using $K_{CB[7]} = 1.00 \times 10^8$ dm ³ mol ⁻¹ and $\Delta\delta_{lim} = 0.174$ ppm.	6
Figure S5. ¹ H NMR (300 MHz) titration of CAPSO (1.02 x 10 ⁻³ mol dm ⁻³) with (a) 0.00, (b) 0.19, (c) 0.39, (d) 0.59, (e) 0.78, (f) 0.84, (g) 0.92, (h) 1.11, (i) 1.36, and (j) 1.96 equivalents of CB[7] in D ₂ O (pD = 4.75, 0.050 mol dm ⁻³ NaOAc-d ₃ (*))/0.025 mol dm ⁻³ DCI).	7
Figure S6. Plot of complexation-induced shift in the proton resonance H _{2a,6a} for CAPSO (1.02 x 10 ⁻³ mol dm ⁻³) as a function of [CB[7]] in D ₂ O (pD = 4.75, 0.050 mol dm ⁻³ NaOAc-d ₃ /0.025 mol dm ⁻³ DCI). The solid curve is a fit to a 1:1 binding model using $K_{CB[7]} = 6.0 \times 10^7$ dm ³ mol ⁻¹ and $\Delta\delta_{lim} = -0.67$ ppm.	8
Figure S7. ¹ H NMR (300 MHz) titration of CABS (1.02 x 10 ⁻³ mol dm ⁻³) with (a) 0.00, (b) 0.16, (c) 0.38, (d) 0.59, (e) 0.81, (f) 0.88, (g) 1.04, (h) 1.17, (i) 1.55, and (j) 1.97 equivalents of CB[7] in D ₂ O (pD = 4.75, 0.050 mol dm ⁻³ NaOAc-d ₃ (*))/0.025 mol dm ⁻³ DCI).	9
Figure S8. Plot of complexation-induced shift in the proton resonance H _{β,γ} for CABS (1.02 x 10 ⁻³ mol dm ⁻³) as a function of [CB[7]] in D ₂ O (pD = 4.75, 0.050 mol dm ⁻³ NaOAc-d ₃ /0.025 mol dm ⁻³ DCI). The solid curve is a fit to a 1:1 binding model using $K_{CB[7]} = 6.0 \times 10^7$ dm ³ mol ⁻¹ and $\Delta\delta_{lim} = +0.15$ ppm.	10
Figure S9. Limiting CB[7] complexation-induced chemical shift changes ($\Delta\delta_{lim}$, ppm) for the proton resonances of the morphilino buffers in D ₂ O (pD = 4.75, 0.050 mol dm ⁻³ NaOAc-d ₃ /0.025 mol dm ⁻³ DCI).	11
Figure S10. ¹ H NMR (300 MHz) titration of MES (1.01 x 10 ⁻³ mol dm ⁻³) with (a) 0.00, (b) 0.25, (c) 0.51, (d) 0.77, (e) 1.03, (f) 1.13, (g) 1.32, (h) 1.65, (i) 1.99, (j) 2.20, (k) 2.49, (l) 2.65, (m) 3.92, (n) 6.05, and (o) 9.08 equivalents of CB[7] in D ₂ O (pD = 4.75, 0.050 mol dm ⁻³ NaOAc-d ₃ (*))/0.025 mol dm ⁻³ DCI).	12
Figure S11. Double reciprocal (Benesi-Hildebrand) plot of $-\Delta\delta^{-1}$ (H _{3,5} resonance) against [CB[7]] ⁻¹	

for the complexation of MES (1.01×10^3 mol dm⁻³) with CB[7] in D₂O (pD = 4.75, 0.050 mol dm⁻³ NaOAc-d₃/0.025 mol dm⁻³ DCI). The linear regression gives $K_{CB[7]} = 213$ dm³ mol⁻¹ from the intercept/slope.

13

Figure S12. ¹H NMR (300 MHz) titration of MOPS (0.956×10^{-3} mol dm⁻³) with (a) 0.00, (b) 0.18, (c) 0.38, (d) 0.60, (e) 0.79, (f) 0.85, (g) 1.01, (h) 1.14, (i) 1.51, (j) 2.11, (k) 3.06, (l) 4.61 and (m) 5.23 equivalents of CB[7] in D₂O (pD = 4.75, 0.050 mol dm⁻³ NaOAc-d₃(*))/0.025 mol dm⁻³ DCI).

14

Figure S13. Plot of complexation-induced shift (-Δδ) in the proton resonance H_α for MOPS (0.956×10^{-3} mol dm⁻³) as a function of [CB[7]] in D₂O (pD = 4.75, 0.050 mol dm⁻³ NaOAc-d₃/0.025 mol dm⁻³ DCI). The solid curve is a fit to a 1:1 binding model using $K_{CB[7]} = 2.27 \times 10^3$ dm³ mol⁻¹ and Δδ_{lim} = -0.25 ppm.

15

Figure S14. ¹H NMR (300 MHz) titration of MOPSO (0.977×10^{-3} mol dm⁻³) with (a) 0.00, (b) 0.21, (c) 0.45, (d) 0.68, (e) 0.98, (f) 1.11, (g) 1.26, (h) 1.49, (i) 1.82, (j) 2.27, (k) 2.52, (l) 2.99 and (m) 4.30 equivalents of CB[7] in D₂O (pD = 4.75, 0.050 mol dm⁻³ NaOAc-d₃(*))/0.025 mol dm⁻³ DCI).

16

Figure S15. Double reciprocal (Benesi-Hildebrand) plot of Δδ⁻¹ against [CB[7]]⁻¹ for the complexation of MOPSO (0.977×10^{-3} mol dm⁻³) in D₂O (pD = 4.75, 0.050 mol dm⁻³ NaOAc-d₃/0.025 mol dm⁻³ DCI). The linear regression gives $K_{CB[7]} = 250$ dm³ mol⁻¹ from the intercept/slope.

17

Figure S16. ¹H NMR (300 MHz) titration of MOBS (0.985×10^{-3} mol dm⁻³) with (a) 0.00, (b) 0.19, (c) 0.44, (d) 0.61, (e) 0.84, (f) 0.94, (g) 1.11, (h) 1.20, (i) 1.47, (j) 2.03, (k) 2.30, (l) 2.62 and (m) 5.09 equivalents of CB[7] in D₂O (pD = 4.75, 0.050 mol dm⁻³ NaOAc-d₃(*))/0.025 mol dm⁻³ DCI).

18

Figure S17. Plot of complexation-induced shift in the proton resonance H_{3,5} for MOBS (0.985×10^{-3} mol dm⁻³) as a function of [CB[7]] in D₂O (pD = 4.75, 0.050 mol dm⁻³ NaOAc-d₃/0.025 mol dm⁻³ DCI). The solid curve is a fit to a 1:1 binding model using $K_{CB[7]} = 2.4 \times 10^3$ dm³ mol⁻¹ and Δδ_{lim} = -0.85 ppm.

19

Figure S18. ¹H NMR (300 MHz) titration of MeMOBS (0.956×10^{-3} mol dm⁻³) with (a) 0.00, (b) 0.21, (c) 0.43, (d) 0.60, (e) 0.79, (f) 0.86, (g) 1.01, (h) 1.17, (i) 1.51, (j) 1.78, (k) 2.40, (l) 2.56, and (m) 4.71 equivalents of CB[7] in D₂O (pD = 4.75, 0.050 mol dm⁻³ NaOAc-d₃(*))/0.025 mol dm⁻³ DCI).

20

Figure S19. Plot of complexation-induced shift in the methyl proton resonance for MeMOBS (1.01×10^{-3} mol dm⁻³) as a function of [CB[7]] in D₂O (pD = 4.75, 0.050 mol dm⁻³ NaOAc-d₃/0.025 mol dm⁻³ DCI). The solid curve is a fit to a 1:1 binding model using $K_{CB[7]} = 4.22 \times 10^4$ dm³ mol⁻¹ and Δδ_{lim} = -0.83 ppm.

21

Figure S20. Limiting CB[7] complexation-induced chemical shift changes (Δδ_{lim}, ppm) for the proton resonances of the piperizino buffers in D₂O (pD = 4.75, 0.050 mol dm⁻³ NaOAc-d₃/0.025 mol dm⁻³ DCI).

22

Figure S21. ¹H NMR (400 MHz) titration of HEPES (1.01×10^{-3} mol dm⁻³) with (a) 0.00, (b) 0.20, (c) 0.40, (d) 0.61, (e) 0.81, (f) 0.91, (g) 1.01, (h) 1.21, (i) 1.51, (j) 2.02, (k) 2.52, (l) 3.03, and (m) 4.61 equivalents of CB[7] in D₂O (pD = 4.75, 0.050 mol dm⁻³ NaOAc-d₃(*))/0.025 mol dm⁻³ DCI).

23

Figure S22. Plot of complexation-induced shift in the H_α proton resonance for HEPES (1.01×10^{-3} mol dm⁻³) as a function of [CB[7]] in D₂O (pD = 4.75, 0.050 mol dm⁻³ NaOAc-d₃/0.025 mol dm⁻³ DCI). The solid curve is a fit to a 1:1 binding model using $K_{CB[7]} = 2.32 \times 10^3$ dm³ mol⁻¹ and Δδ_{lim} = 0.43 ppm.

24

Figure S23. ¹H NMR (400 MHz) spectra for the complexation of EPPS (1.03×10^3 mol dm⁻³) with (a) 0.00, (b) 0.21, (c) 0.43, (d) 0.61, (e) 0.75, (f) 0.85, (g) 1.01, (h) 1.25, (i) 1.49, (j) 1.91, and (k) 4.80 equivalents of CB[7] in D₂O (pD = 4.75, 0.050 mol dm⁻³ NaOAc-d₃(*))/0.025 mol dm⁻³ DCI).

25

Figure S24. Plot of complexation-induced shift in the proton resonance H_α for EPPS (1.03×10^{-3} mol dm⁻³) as a function of [CB[7]] in D₂O (pD = 4.75, 0.050 mol dm⁻³ NaOAc-d₃/0.025 mol dm⁻³ DCI). The solid curve is a fit to a 1:1 binding model using $K_{CB[7]} = 8.86 \times 10^3$ dm³ mol⁻¹ and Δδ_{lim} = 0.27 ppm.

26

- Figure S25.** ^1H NMR (300 MHz) titration of HEPBS (0.976×10^{-3} mol dm $^{-3}$) with (a) 0.00, (b) 0.23, (c) 0.45, (d) 0.68, (e) 0.79, (f) 0.90, (g) 1.01, (h) 1.13, (i) 1.35, (j) 1.69, (k) 2.26, (l) 2.82 and (m) 3.39 equivalents of CB[7] in D₂O (pD = 4.75, 0.050 mol dm $^{-3}$ NaOAc-d₃(*)/0.025 mol dm $^{-3}$ DCI). 27
- Figure S26.** Plot of complexation-induced shift in the proton resonance H δ for HEPBS (0.976×10^{-3} mol dm $^{-3}$) as a function of [CB[7]] in D₂O (pD = 4.75, 0.050 mol dm $^{-3}$ NaOAc-d₃/0.025 mol dm $^{-3}$ DCI). The solid curve is a fit to a 1:1 binding model using $K_{\text{CB}[7]} = 2.1 \times 10^4$ dm 3 mol $^{-1}$ and $\Delta\delta_{\text{lim}} = 0.148$ ppm. 28
- Figure S27.** ^1H NMR spectra of PIPES (1.0 mmol dm $^{-3}$) in the absence and presence of 5.0 mmol dm $^{-3}$ CB[7] at pD = 2 (bottom), 5 (middle), and 12 (top). 29
- Figure S28.** ^1H NMR spectra of PIPPS (1.0 mmol dm $^{-3}$) in the absence and presence of 5.0 mmol dm $^{-3}$ CB[7] at pD = 1 (bottom), 5 (middle), and 11 (top). 30
- Figure S29.** ^1H NMR (300 MHz) titration of PIPBS (0.948×10^{-3} mol dm $^{-3}$) with (a) 0.00, (b) 0.32, (c) 0.64, (d) 0.95, (e) 1.27, (f) 1.43, (g) 1.59, (h) 1.90, (i) 2.38, (j) 3.17, and (k) 8.15 equivalents of CB[7] in D₂O (pD = 4.75, 0.050 mol dm $^{-3}$ NaOAc-d₃(*)/0.025 mol dm $^{-3}$ DCI). 31
- Figure S30.** ^1H NMR (300 MHz) spectra for the complexation of TRIS (1.16×10^3 mol dm $^{-3}$) with (a) 0.00, (b) 0.19, (c) 0.39, (d) 0.60, (e) 0.79, (f) 0.90, (g) 0.98, (h) 1.21, (i) 1.48, (j) 1.97, (k) 2.56, (l) 2.89, (m) 3.22, and (n) 4.31 equivalents of CB[7] in D₂O (pD = 4.75, 0.050 mol dm $^{-3}$ NaOAc-d₃(*)/0.025 mol dm $^{-3}$ DCI). 32
- Figure S31.** Double reciprocal (Benesi-Hildebrand) plot of $\Delta\delta^{-1}$ (H₂) against [CB[7]] $^{-1}$ for the complexation of TRIS (1.16×10^3 mol dm $^{-3}$) with CB[7] in D₂O (pD = 4.75, 0.050 mol dm $^{-3}$ NaOAc-d₃/0.025 mol dm $^{-3}$ DCI). The linear regression gives $K_{\text{CB}[7]} = 291$ dm 3 mol $^{-1}$ from the intercept/slope. 32
- Figure S32.** ^1H NMR (300 MHz) spectra for the complexation of TAPS (0.980×10^3 mol dm $^{-3}$) with (a) 0.00, (b) 0.18, (c) 0.37, (d) 0.57, (e) 0.75, (f) 0.86, (g) 0.90, (h) 1.12, (i) 1.45, (j) 1.87, (k) 2.27, (l) 2.73, (m) 3.31, and (n) 5.23 equivalents of CB[7] in D₂O (pD = 4.75, 0.050 mol dm $^{-3}$ NaOAc-d₃(*)/0.025 mol dm $^{-3}$ DCI). 33
- Figure S33.** Double reciprocal (Benesi-Hildebrand) plot of $\Delta\delta^{-1}$ (H₂) against [CB[7]] $^{-1}$ for the complexation of TAPS (0.980×10^3 mol dm $^{-3}$) with CB[7] in D₂O (pD = 4.75, 0.050 mol dm $^{-3}$ NaOAc-d₃/0.025 mol dm $^{-3}$ DCI). The linear regression gives $K_{\text{CB}[7]} = 113$ dm 3 mol $^{-1}$ from the intercept/slope. 34

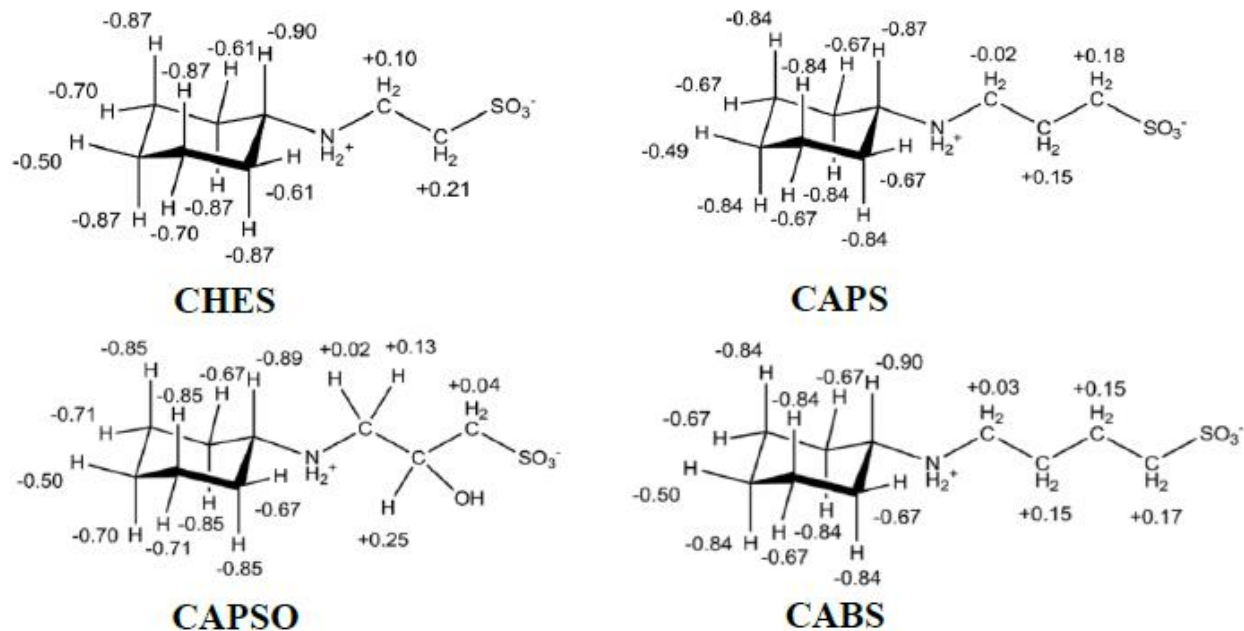


Figure S1. Limiting CB[7] complexation-induced chemical shift changes ($\Delta\delta_{\text{lim}}$, ppm) for the proton resonances of the cyclohexylamino buffers in D_2O ($\text{pD} = 4.75$, $0.050 \text{ mol dm}^{-3}$ NaOAc-d_3 / $0.025 \text{ mol dm}^{-3}$ DCl).

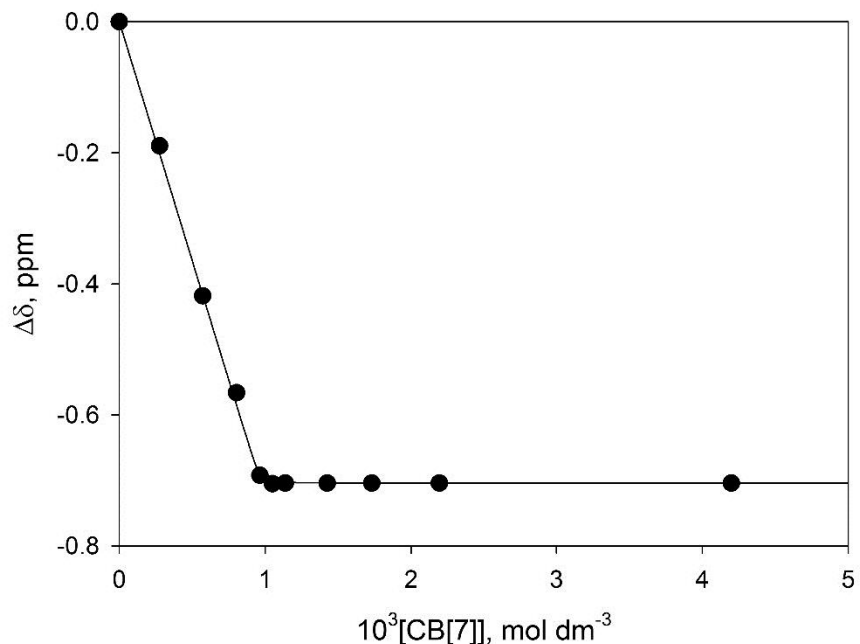


Figure S2. Plot of complexation-induced shift in the proton resonance $\text{H}_{3a,5a}$ for CHES ($0.965 \times 10^{-3} \text{ mol dm}^{-3}$) as a function of $[\text{CB}[7]]$ in D_2O ($\text{pD} = 4.75$, $0.050 \text{ mol dm}^{-3}$ NaOAc-d_3 / $0.025 \text{ mol dm}^{-3}$ DCl). The solid curve is a fit to a 1:1 binding model using $K_{\text{CB}[7]} = 3.60 \times 10^7 \text{ dm}^3 \text{ mol}^{-1}$ and $\Delta\delta_{\text{lim}} = -0.704 \text{ ppm}$.

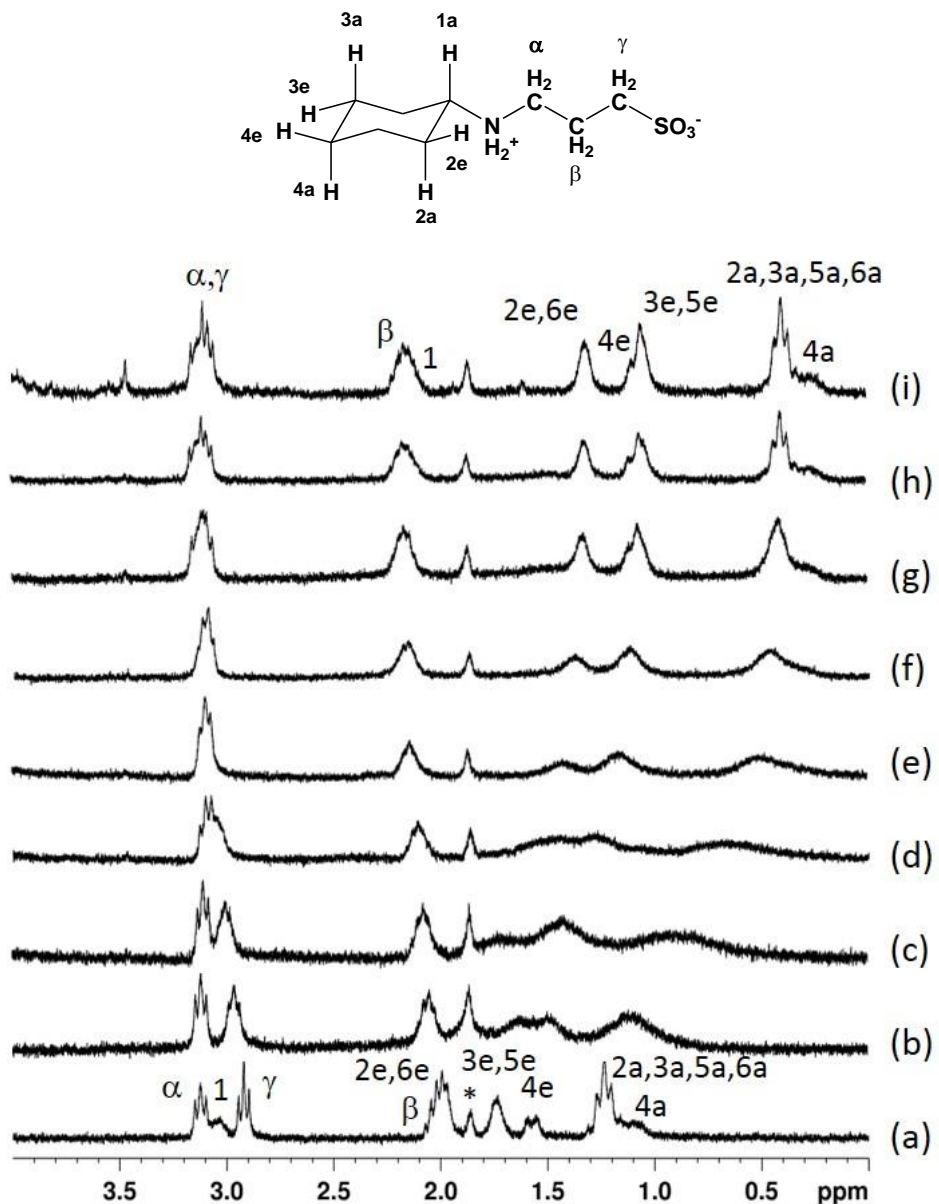


Figure S3. ^1H NMR (300 MHz) titration of CAPS ($1.02 \times 10^{-3} \text{ mol dm}^{-3}$) with (a) 0.00, (b) 0.18, (c) 0.42, (d) 0.60, (e) 0.82, (f) 0.92, (g) 0.98, (h) 1.14, (i) 2.05, and (j) 4.52 equivalents of CB[7] in D_2O ($\text{pD} = 4.75$, $0.050 \text{ mol dm}^{-3}$ NaOAc- d_3 (*)/ $0.025 \text{ mol dm}^{-3}$ DCl).

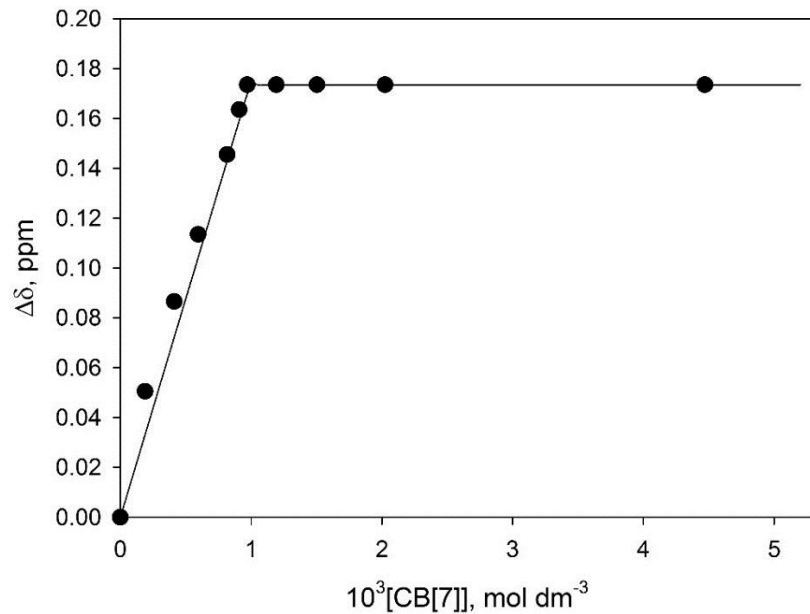


Figure S4. Plot of complexation-induced shift in the proton resonance H γ for CAPS (0.990×10^{-3} mol dm $^{-3}$) as a function of [CB[7]] in D $_2$ O (pD = 4.75, 0.050 mol dm $^{-3}$ NaOAc-d $_3$ /0.025 mol dm $^{-3}$ DCl). The solid curve is a fit to a 1:1 binding model using $K_{\text{CB}[7]} = 1.00 \times 10^8$ dm 3 mol $^{-1}$ and $\Delta\delta_{\text{lim}} = 0.174$ ppm.

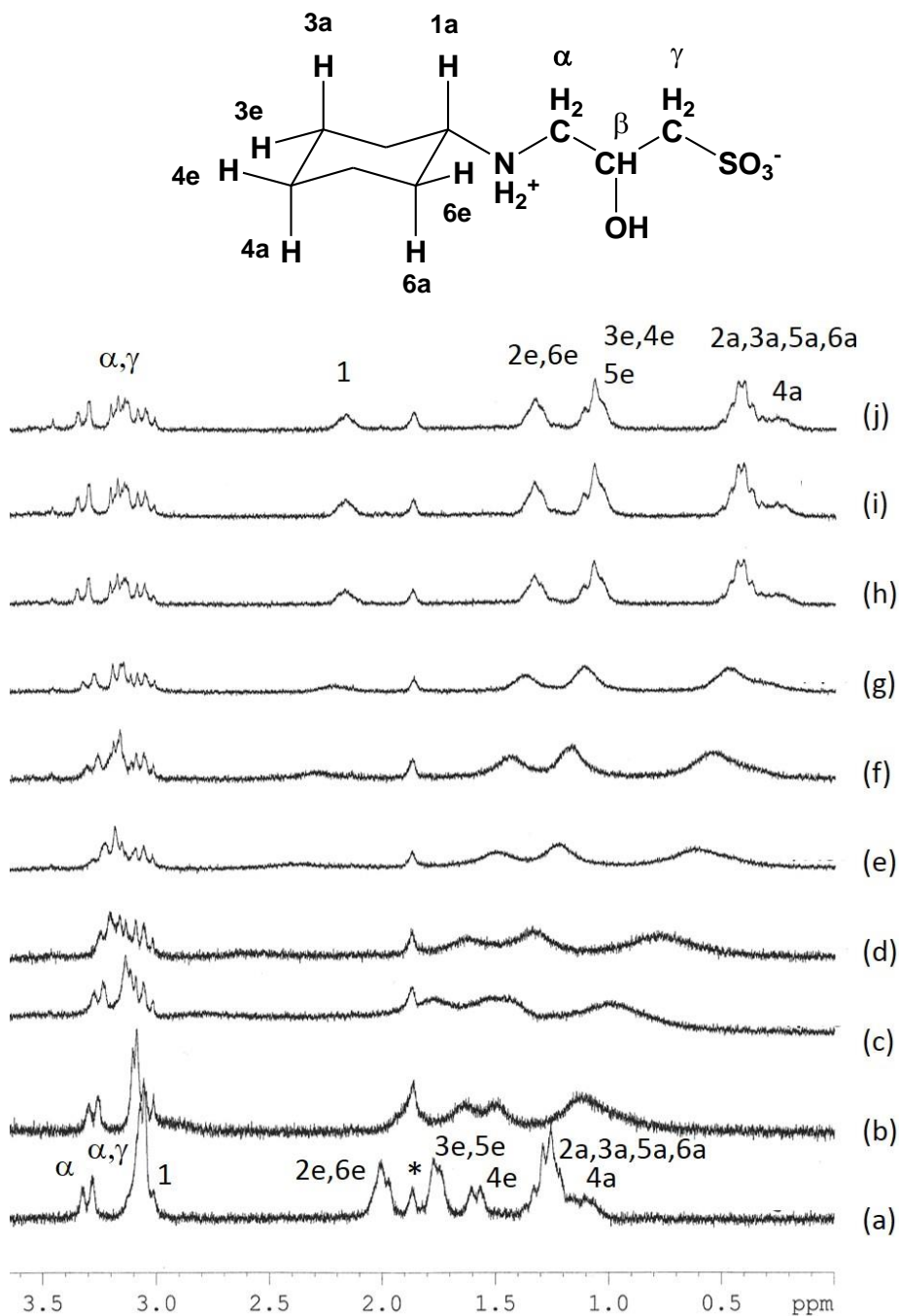


Figure S5. ^1H NMR (300 MHz) titration of CAPSO ($1.02 \times 10^{-3} \text{ mol dm}^{-3}$) with (a) 0.00, (b) 0.19, (c) 0.39, (d) 0.59, (e) 0.78, (f) 0.84, (g) 0.92, (h) 1.11, (i) 1.36, and (j) 1.96 equivalents of CB[7] in D_2O ($\text{pD} = 4.75$, $0.050 \text{ mol dm}^{-3} \text{ NaOAc-d}_3$ (*)/ $0.025 \text{ mol dm}^{-3} \text{ DCl}$).

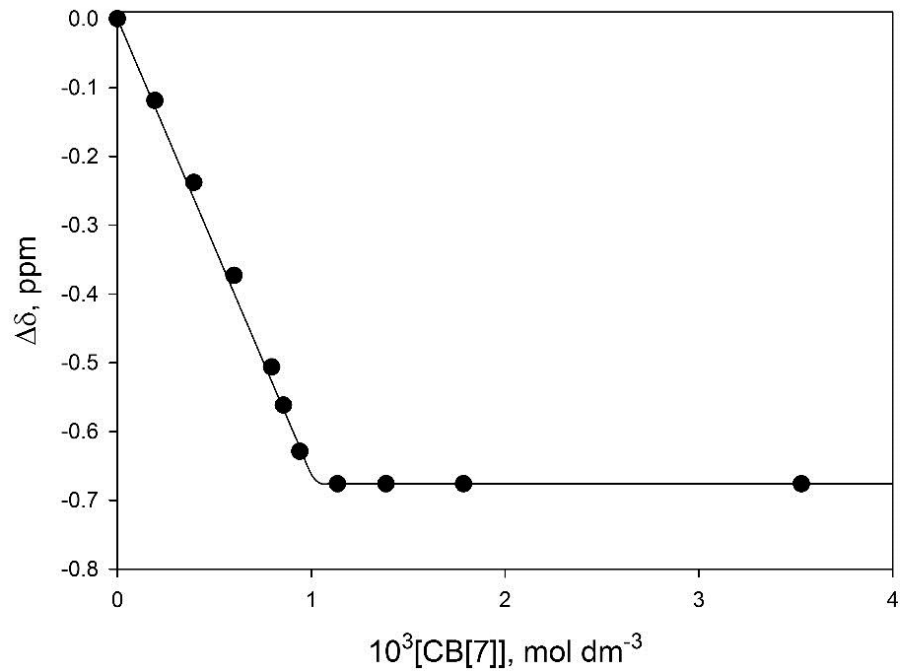


Figure S6. Plot of complexation-induced shift in the proton resonance $H_{2a,6a}$ for CAPSO ($1.02 \times 10^{-3} \text{ mol dm}^{-3}$) as a function of $[CB[7]]$ in D_2O ($pD = 4.75$, $0.050 \text{ mol dm}^{-3}$ NaOAc-d₃/0.025 mol dm⁻³ DCl). The solid curve is a fit to a 1:1 binding model using $K_{CB[7]} = 6.0 \times 10^7 \text{ dm}^3 \text{ mol}^{-1}$ and $\Delta\delta_{\text{lim}} = -0.67 \text{ ppm}$.

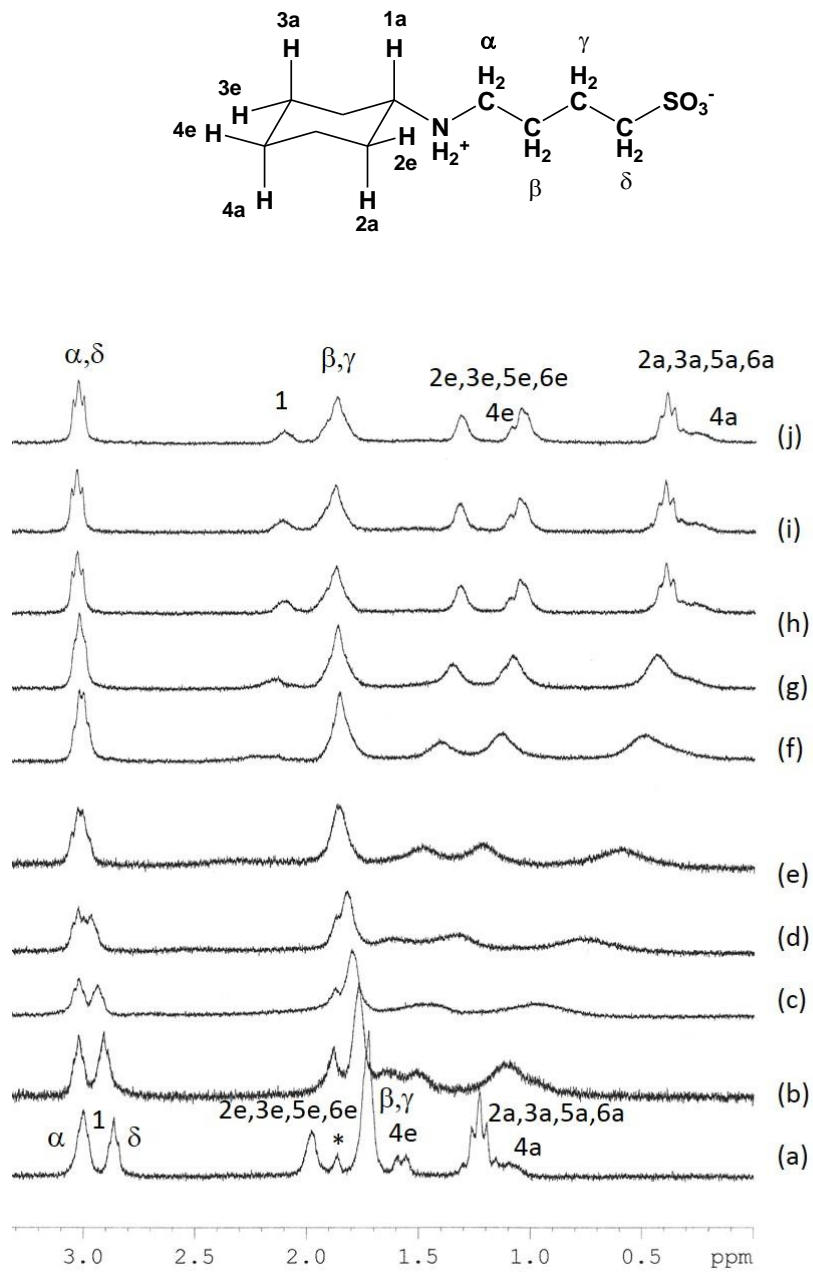


Figure S7. ^1H NMR (300 MHz) titration of CABS (1.02×10^{-3} mol dm $^{-3}$) with (a) 0.00, (b) 0.16, (c) 0.38, (d) 0.59, (e) 0.81, (f) 0.88, (g) 1.04, (h) 1.17, (i) 1.55, and (j) 1.97 equivalents of CB[7] in D₂O (pD = 4.75, 0.050 mol dm $^{-3}$ NaOAc-d₃(*)/0.025 mol dm $^{-3}$ DCl).

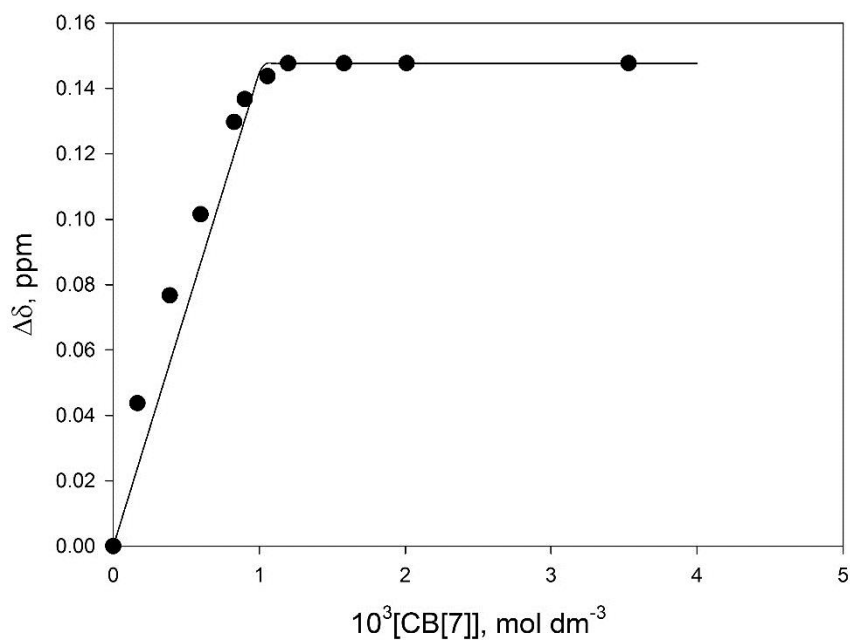


Figure S8. Plot of complexation-induced shift in the proton resonance $H_{\beta,\gamma}$ for CABS (1.02×10^{-3} mol dm⁻³) as a function of [CB[7]] in D₂O (pD = 4.75, 0.050 mol dm⁻³ NaOAc-d₃/0.025 mol dm⁻³ DCl). The solid curve is a fit to a 1:1 binding model using $K_{\text{CB}[7]} = 1.3 \times 10^8 \text{ dm}^3 \text{ mol}^{-1}$ and $\Delta\delta_{\text{lim}} = +0.15 \text{ ppm}$.

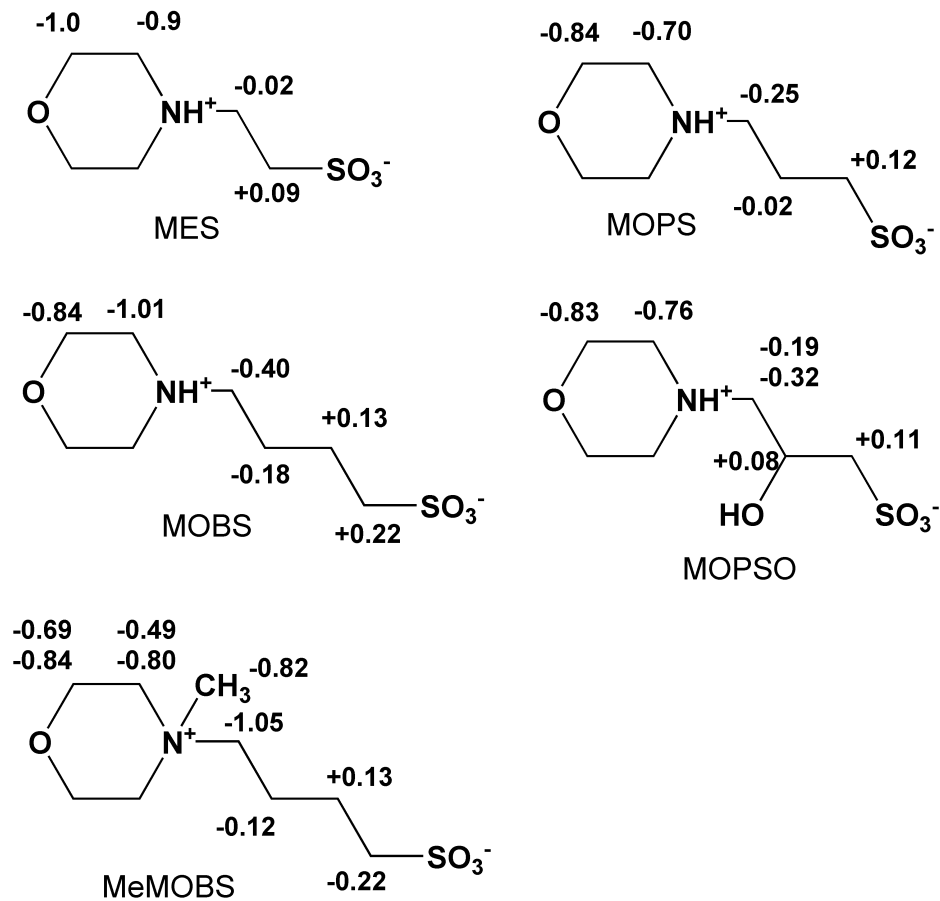


Figure S9. Limiting CB[7] complexation-induced chemical shift changes ($\Delta\delta_{\text{lim}}$, ppm) for the proton resonances of the morphilino buffers in D_2O ($\text{pD} = 4.75$, $0.050 \text{ mol dm}^{-3} \text{ NaOAc-d}_3/0.025 \text{ mol dm}^{-3} \text{ DCl}$).

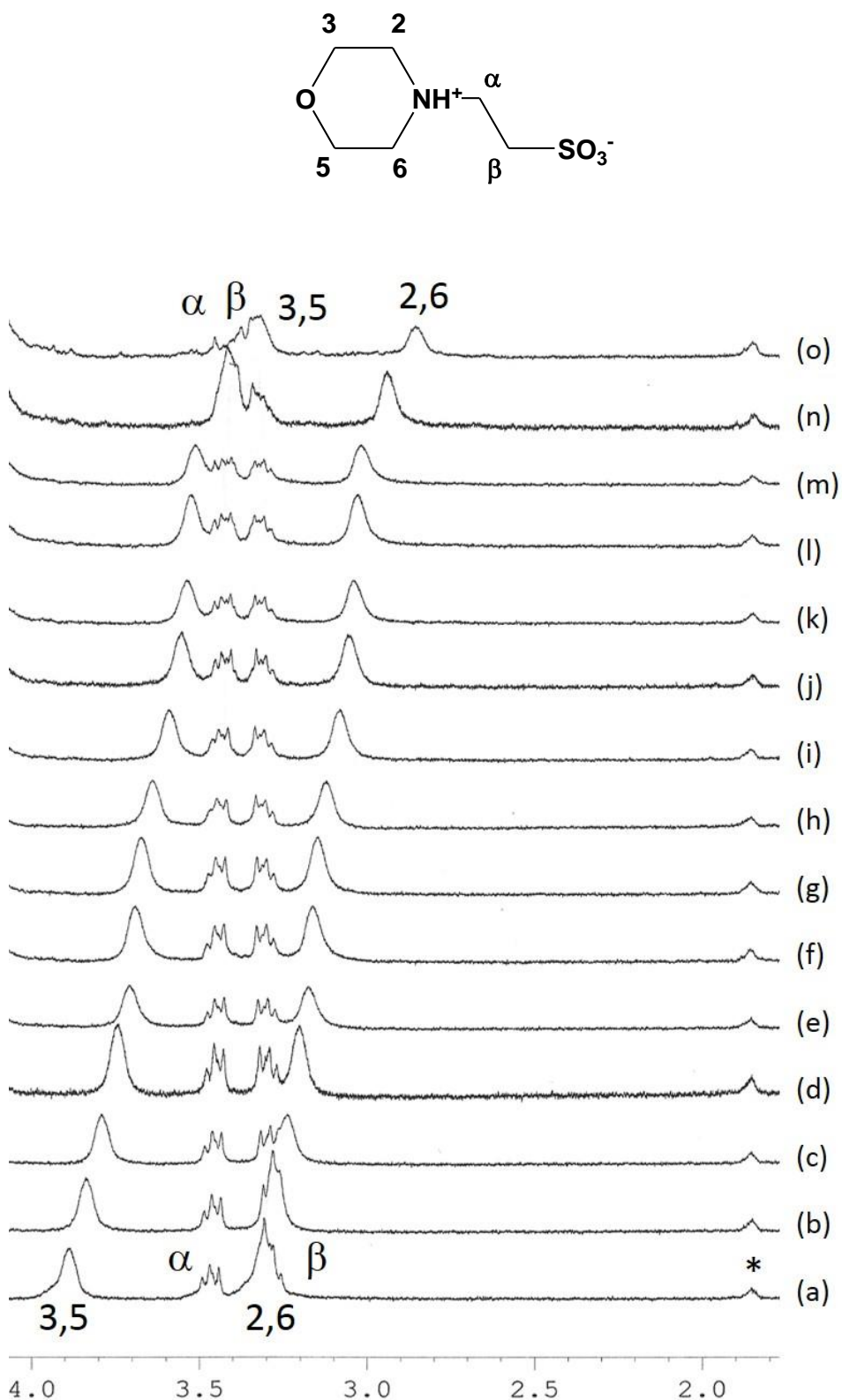


Figure S10. ^1H NMR (300 MHz) titration of MES (1.01×10^{-3} mol dm $^{-3}$) with (a) 0.00, (b) 0.25, (c) 0.51, (d) 0.77, (e) 1.03, (f) 1.13, (g) 1.32, (h) 1.65, (i) 1.99, (j) 2.20, (k) 2.49, (l) 2.65, (m) 3.92, (n) 6.05, and (o) 9.08 equivalents of CB[7] in D₂O (pD = 4.75, 0.050 mol dm $^{-3}$ NaOAc-d₃(*))/0.025 mol dm $^{-3}$ DCl).

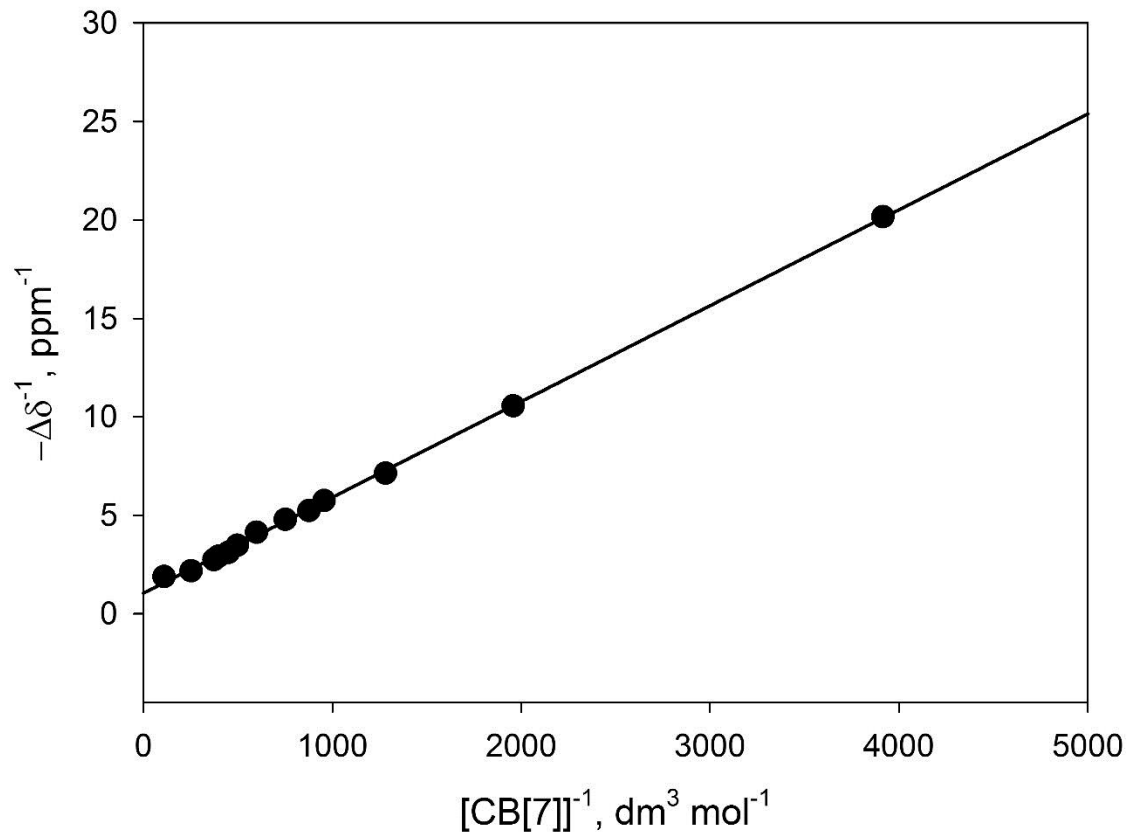


Figure S11. Double reciprocal (Benesi-Hildebrand) plot of $-\Delta\delta^{-1}$ ($H_{3,5}$ resonance) against $[CB[7]]^{-1}$ for the complexation of MES (1.01×10^3 mol dm⁻³) with CB[7] in D₂O (pD = 4.75, 0.050 mol dm⁻³ NaOAc-d₃/0.025 mol dm⁻³ DCl). The linear regression gives $K_{CB[7]} = 213$ dm³ mol⁻¹ from the intercept/slope.

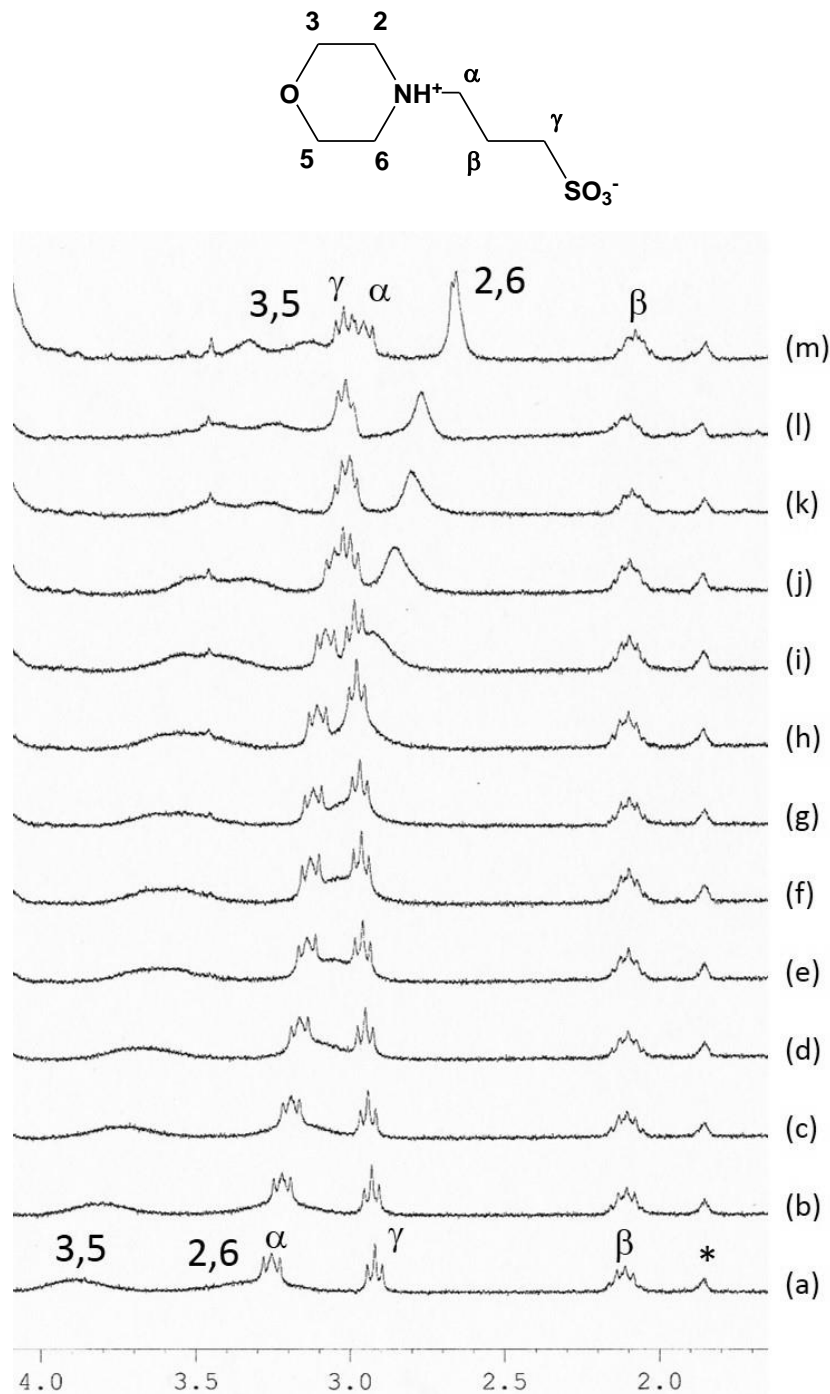


Figure S12. ${}^1\text{H}$ NMR (300 MHz) titration of MOPS (0.956×10^{-3} mol dm $^{-3}$) with (a) 0.00, (b) 0.18, (c) 0.38, (d) 0.60, (e) 0.79, (f) 0.85, (g) 1.01, (h) 1.14, (i) 1.51, (j) 2.11, (k) 3.06, (l) 4.61 and (m) 5.23 equivalents of CB[7] in D₂O (pD = 4.75, 0.050 mol dm $^{-3}$ NaOAc-d₃(*)/0.025 mol dm $^{-3}$ DCI).

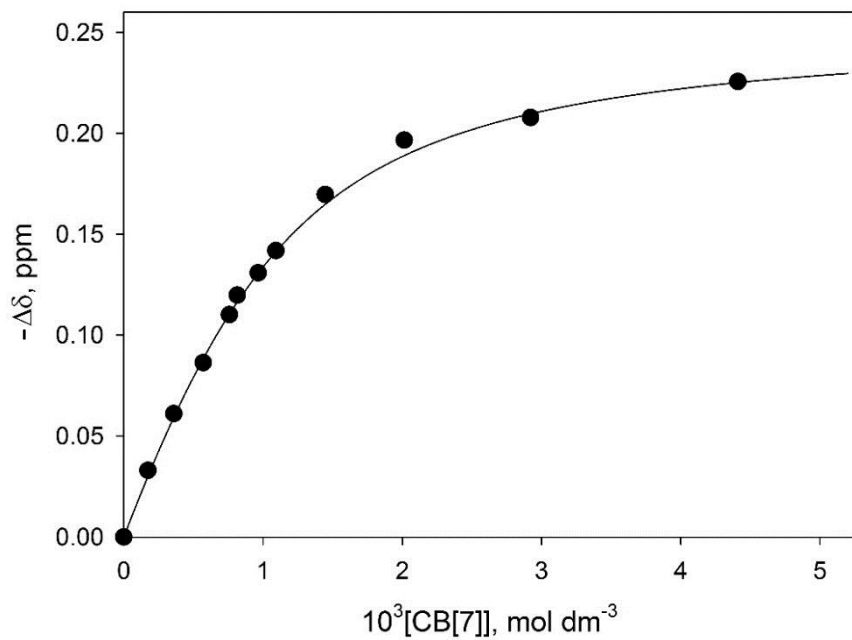


Figure S13. Plot of complexation-induced shift ($-\Delta\delta$) in the proton resonance $\text{H}\alpha$ for MOPS (0.956×10^{-3} mol dm⁻³) as a function of [CB[7]] in D₂O (pD = 4.75, 0.050 mol dm⁻³ NaOAc-d₃/0.025 mol dm⁻³ DCl). The solid curve is a fit to a 1:1 binding model using $K_{\text{CB}[7]} = 2.2 \times 10^3$ dm³ mol⁻¹ and $\Delta\delta_{\text{lim}} = -0.25$ ppm.

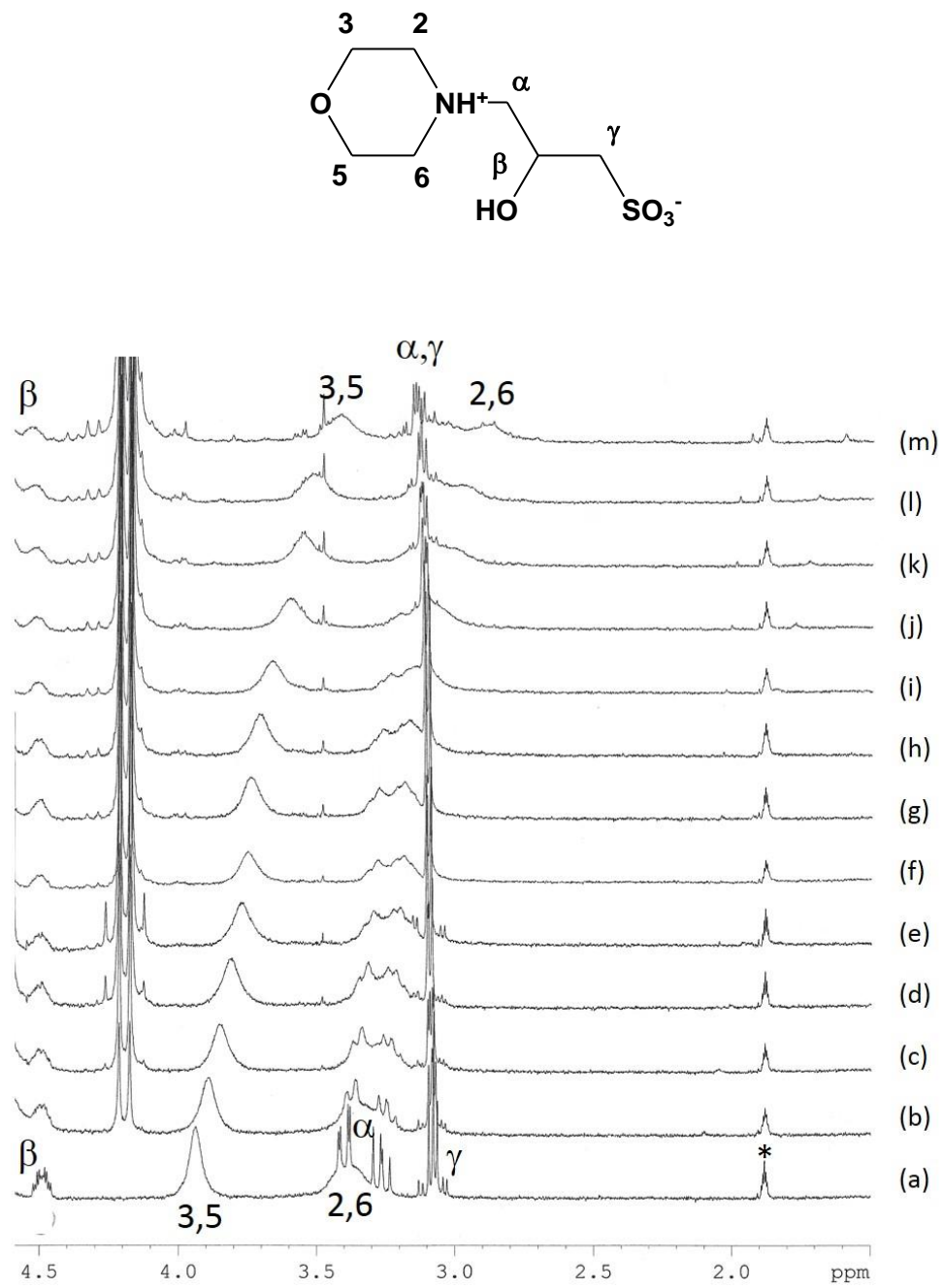


Figure S14. ^1H NMR (300 MHz) titration of MOPSO ($0.977 \times 10^{-3} \text{ mol dm}^{-3}$) with (a) 0.00, (b) 0.21, (c) 0.45, (d) 0.68, (e) 0.98, (f) 1.11, (g) 1.26, (h) 1.49, (i) 1.82, (j) 2.27, (k) 2.52, (l) 2.99 and (m) 4.30 equivalents of CB[7] in D_2O ($\text{pD} = 4.75$, $0.050 \text{ mol dm}^{-3}$ NaOAc-d_3 (*)/ $0.025 \text{ mol dm}^{-3}$ DCl).

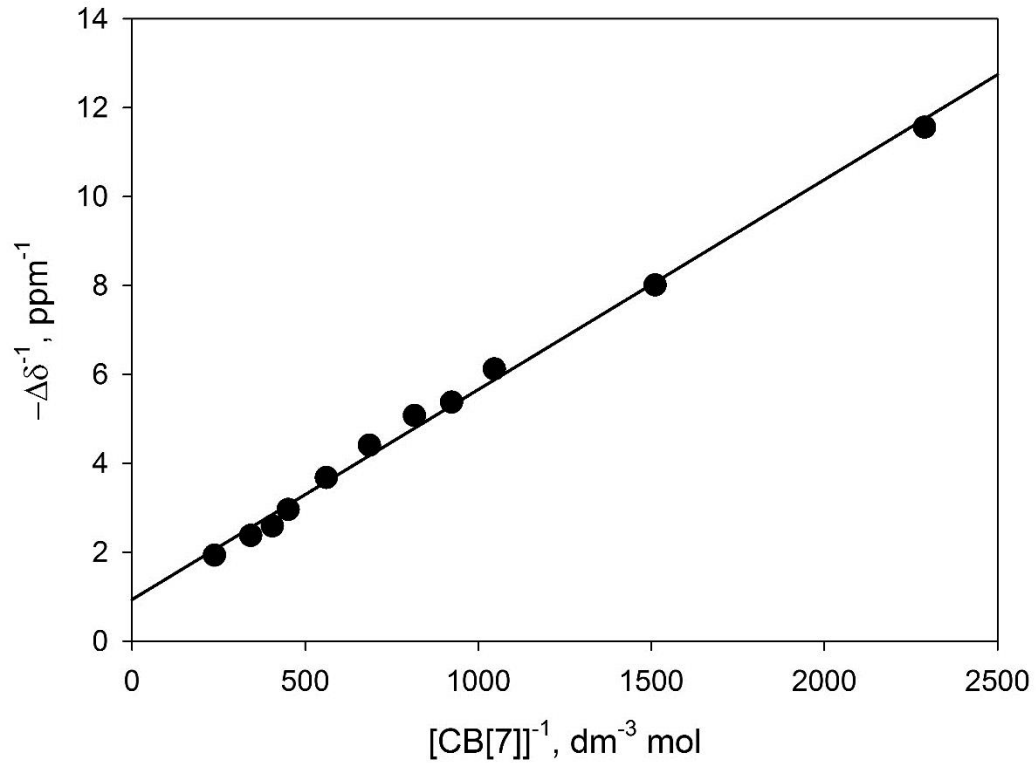


Figure S15. Double reciprocal (Benesi-Hildebrand) plot of $\Delta\delta^{-1}$ against $[CB[7]]^{-1}$ for the complexation of MOPSO (0.977×10^{-3} mol dm⁻³) in D₂O (pD = 4.75, 0.050 mol dm⁻³ NaOAc-d₃/0.025 mol dm⁻³ DCl). The linear regression gives $K_{CB[7]} = 330$ dm³ mol⁻¹ from the intercept/slope.

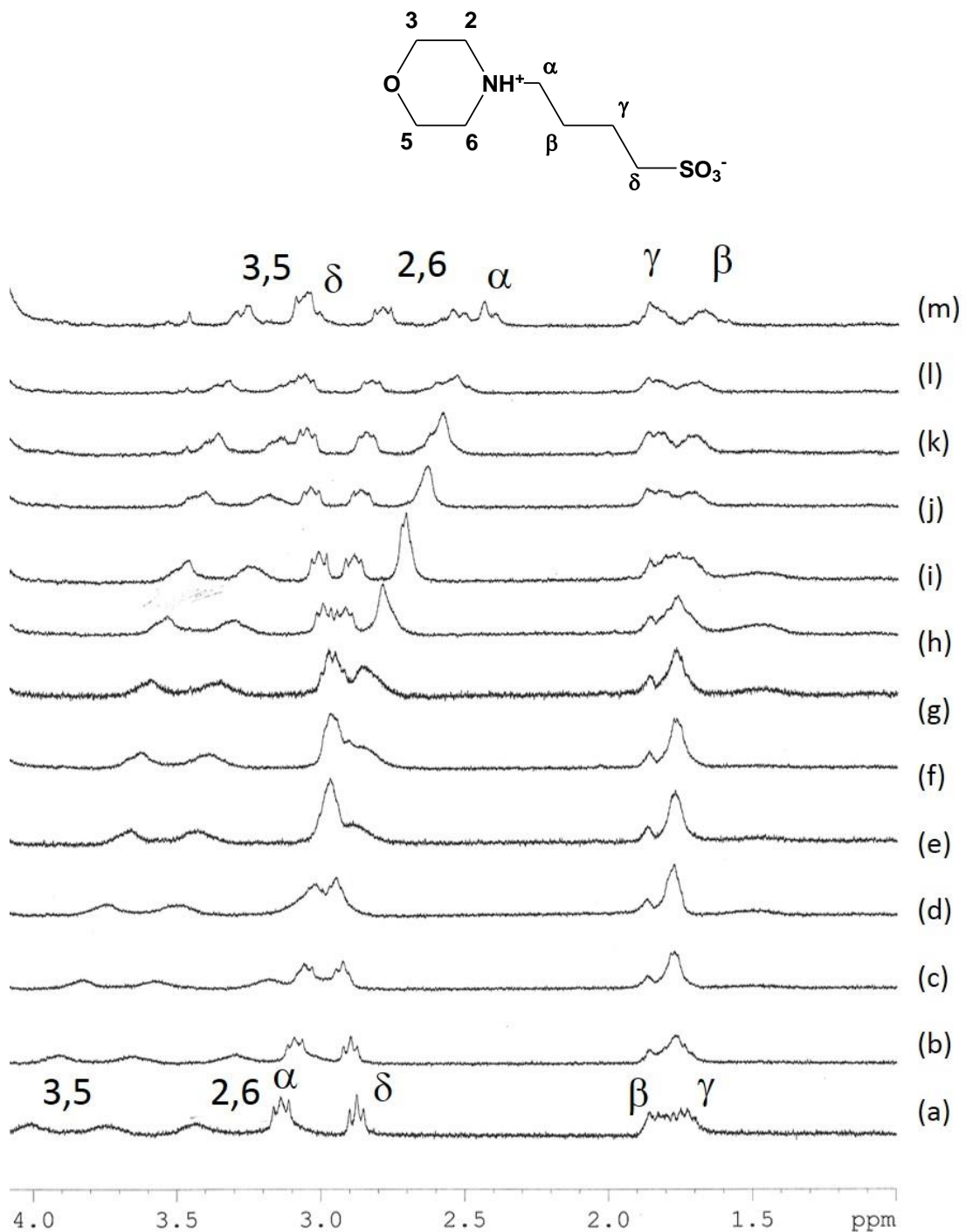


Figure S16. ^1H NMR (300 MHz) titration of MOBS ($0.985 \times 10^{-3} \text{ mol dm}^{-3}$) with (a) 0.00, (b) 0.19, (c) 0.44, (d) 0.61, (e) 0.84, (f) 0.94, (g) 1.11, (h) 1.20, (i) 1.47, (j) 2.03, (k) 2.30, (l) 2.62 and (m) 5.09 equivalents of CB[7] in D_2O ($\text{pD} = 4.75$, $0.050 \text{ mol dm}^{-3}$ $\text{NaOAc-d}_3(*)/0.025 \text{ mol dm}^{-3}$ DCl).

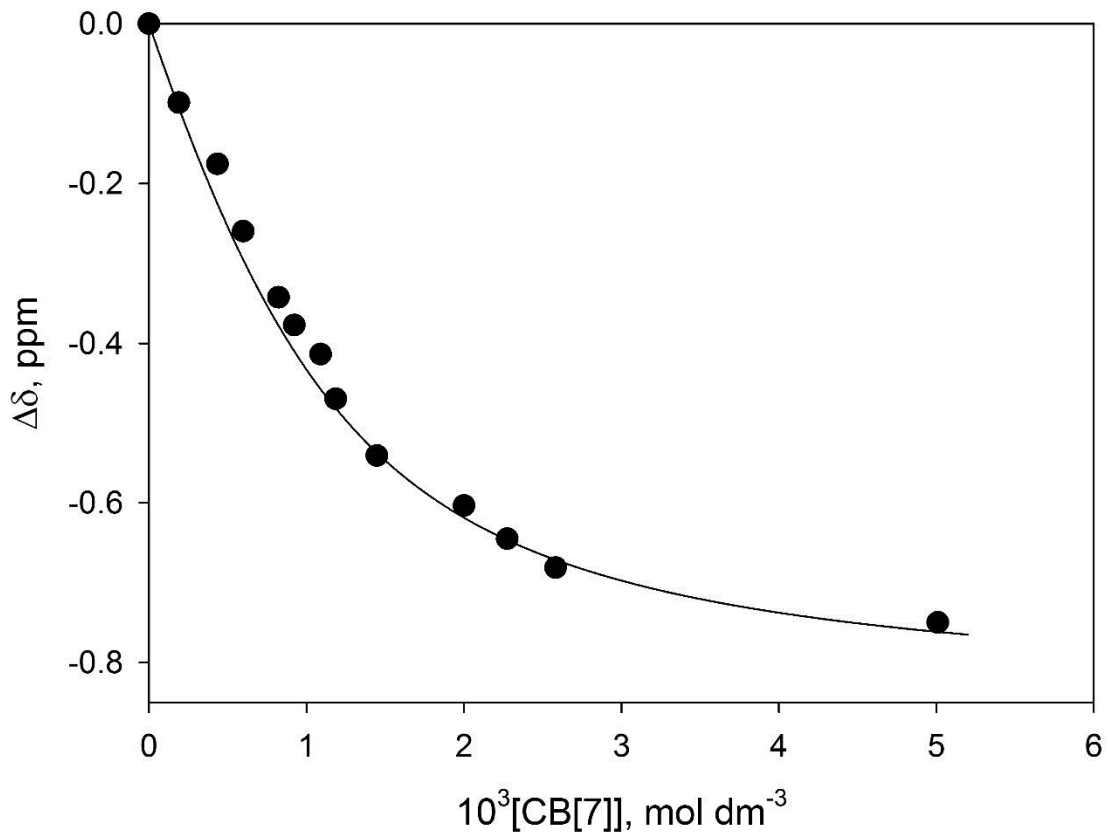


Figure S17. Plot of complexation-induced shift in the proton resonance $\text{H}_{3,5}$ for MOBS ($0.985 \times 10^{-3} \text{ mol dm}^{-3}$) as a function of $[\text{CB}[7]]$ in D_2O ($\text{pD} = 4.75$, $0.050 \text{ mol dm}^{-3}$ NaOAc-d_3 / $0.025 \text{ mol dm}^{-3}$ DCl). The solid curve is a fit to a 1:1 binding model using $K_{\text{CB}[7]} = 2.4 \times 10^3 \text{ dm}^3 \text{ mol}^{-1}$ and $\Delta\delta_{\text{lim}} = -0.84 \text{ ppm}$.

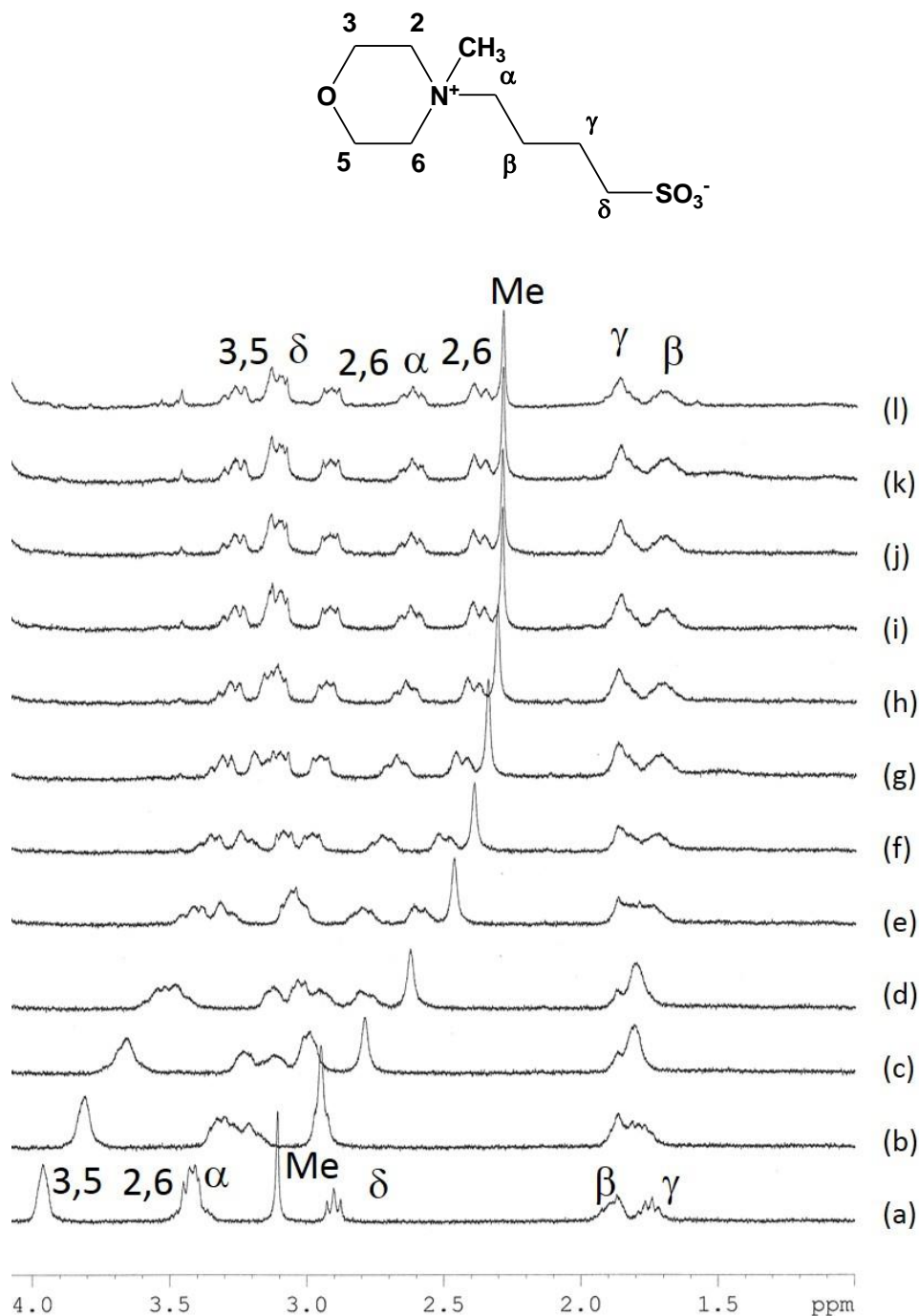


Figure S18. ^1H NMR (300 MHz) titration of MeMOBS ($0.956 \times 10^{-3} \text{ mol dm}^{-3}$) with (a) 0.00, (b) 0.21, (c) 0.43, (d) 0.60, (e) 0.79, (f) 0.86, (g) 1.01, (h) 1.17, (i) 1.51, (j) 1.78, (k) 2.40, (l) 2.56, and (m) 4.71 equivalents of CB[7] in D_2O ($\text{pD} = 4.75$, $0.050 \text{ mol dm}^{-3}$ $\text{NaOAc-d}_3(*)/0.025 \text{ mol dm}^{-3}$ DCl).

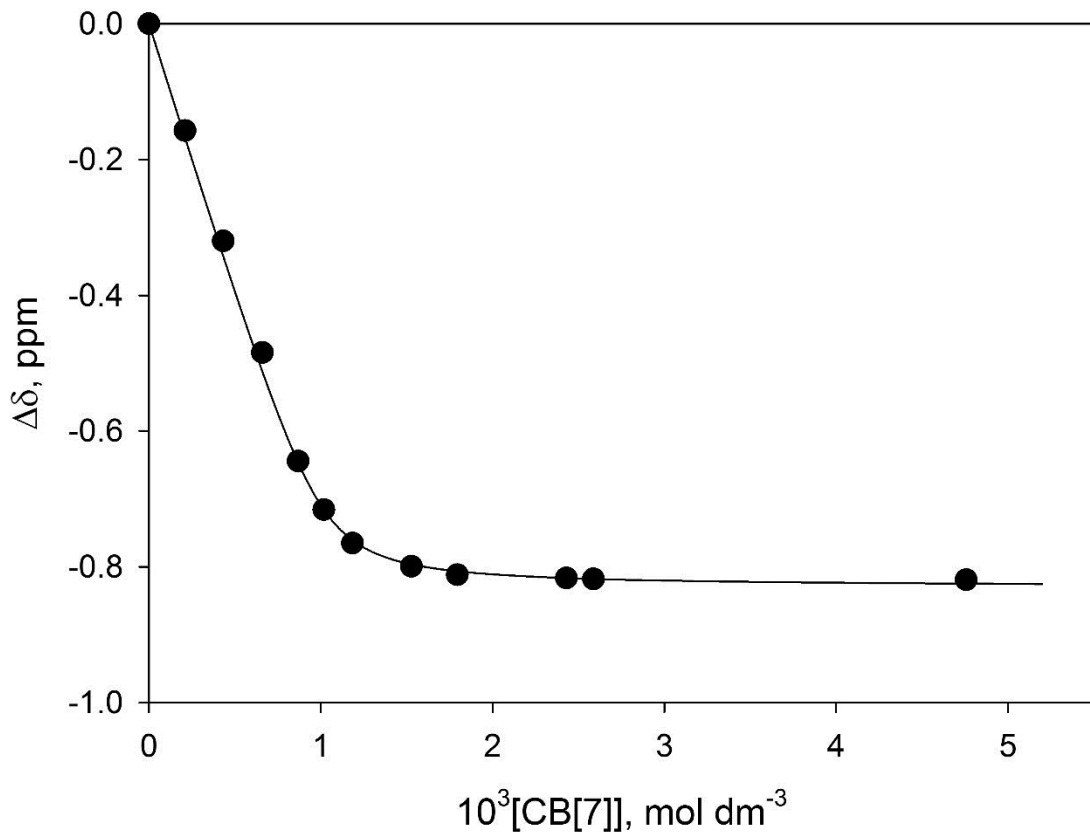


Figure S19. Plot of complexation-induced shift in the methyl proton resonance for MeMOBS ($1.01 \times 10^{-3} \text{ mol dm}^{-3}$) as a function of $[\text{CB}[7]]$ in D_2O ($\text{pD} = 4.75$, $0.050 \text{ mol dm}^{-3} \text{ NaOAc-d}_3/0.025 \text{ mol dm}^{-3} \text{ DCl}$). The solid curve is a fit to a 1:1 binding model using $K_{\text{CB}[7]} = 4.22 \times 10^4 \text{ dm}^3 \text{ mol}^{-1}$ and $\Delta\delta_{\text{lim}} = -0.83 \text{ ppm}$.

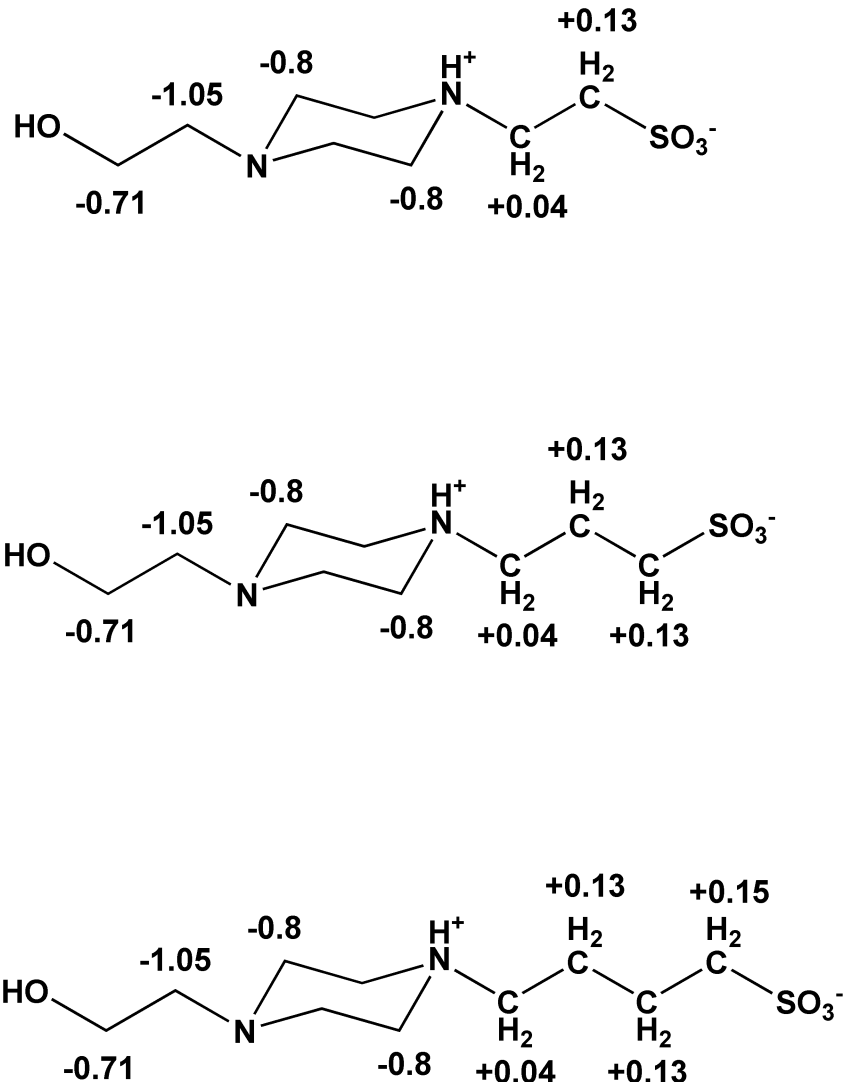


Figure S20. Limiting CB[7] complexation-induced chemical shift changes ($\Delta\delta_{\text{lim}}$, ppm) for the proton resonances of the piperazine buffers in D₂O (pD = 4.75, 0.050 mol dm⁻³ NaOAc-d₃/0.025 mol dm⁻³ DCl).

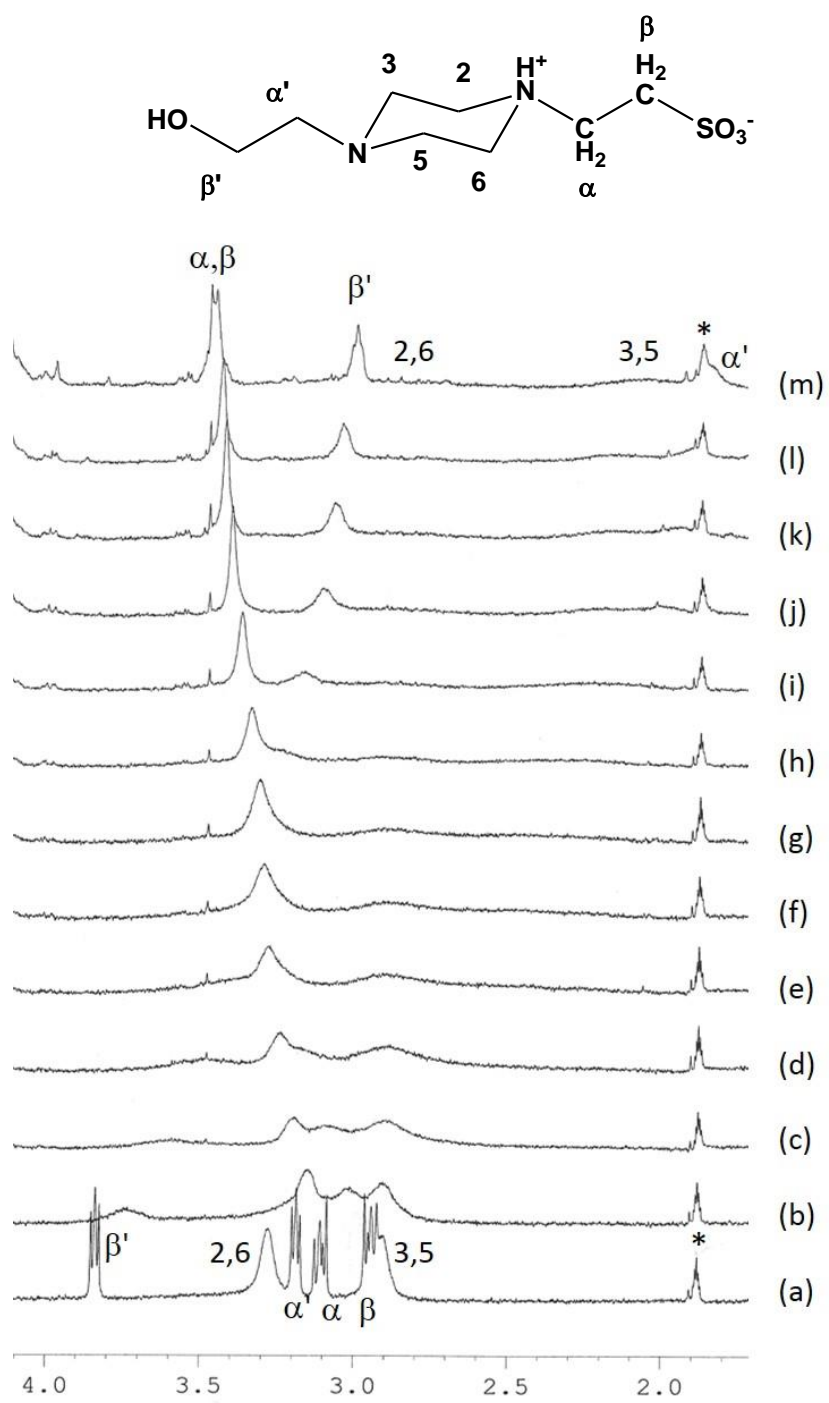


Figure S21. ^1H NMR (400 MHz) titration of HEPES ($1.01 \times 10^{-3} \text{ mol dm}^{-3}$) with (a) 0.00, (b) 0.20, (c) 0.40, (d) 0.61, (e) 0.81, (f) 0.91, (g) 1.01, (h) 1.21, (i) 1.51, (j) 2.02, (k) 2.52, (l) 3.03, and (m) 4.61 equivalents of CB[7] in D₂O (pD = 4.75, 0.050 mol dm⁻³ NaOAc-d₃(*)/0.025 mol dm⁻³ DCl).

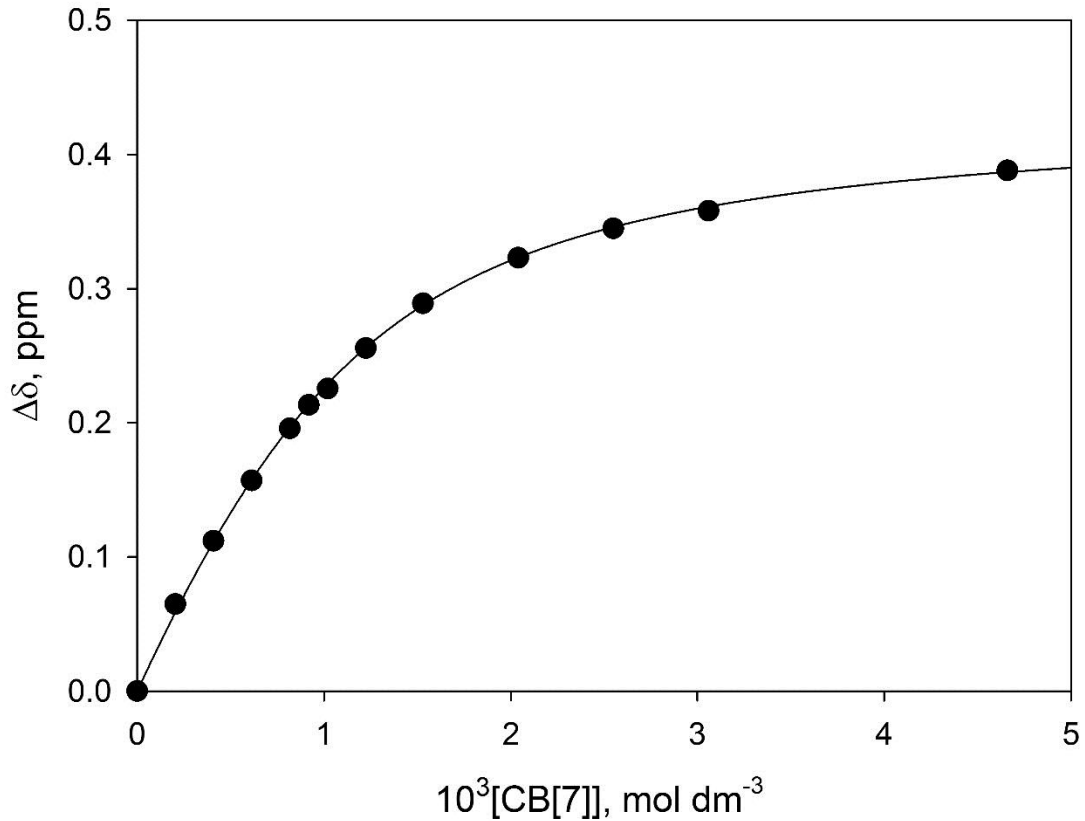


Figure S22. Plot of complexation-induced shift in the H α proton resonance for HEPES (1.01×10^{-3} mol dm $^{-3}$) as a function of [CB[7]] in D₂O (pD = 4.75, 0.050 mol dm $^{-3}$ NaOAc-d₃/0.025 mol dm $^{-3}$ DCI). The solid curve is a fit to a 1:1 binding model using $K_{\text{CB}[7]} = 2.32 \times 10^3 \text{ dm}^3 \text{ mol}^{-1}$ and $\Delta\delta_{\text{lim}} = 0.43 \text{ ppm}$.

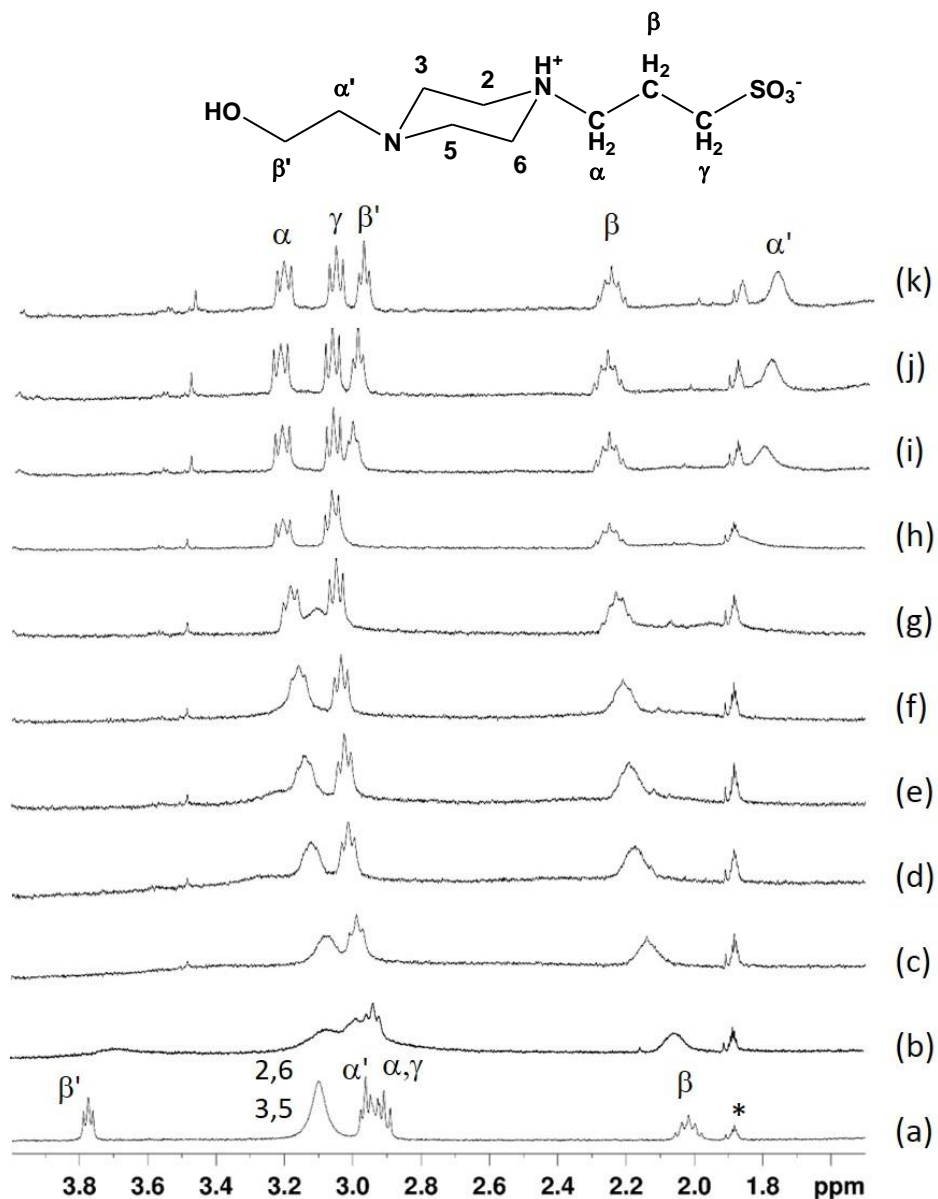


Figure S23. ^1H NMR (400 MHz) spectra for the complexation of EPPS (1.03×10^{-3} mol dm $^{-3}$) with (a) 0.00, (b) 0.21, (c) 0.43, (d) 0.61, (e) 0.75, (f) 0.85, (g) 1.01, (h) 1.25, (i) 1.49, (j) 1.91, and (k) 4.80 equivalents of CB[7] in D₂O (pD = 4.75, 0.050 mol dm $^{-3}$ NaOAc-d₃(*))/0.025 mol dm $^{-3}$ DCl).

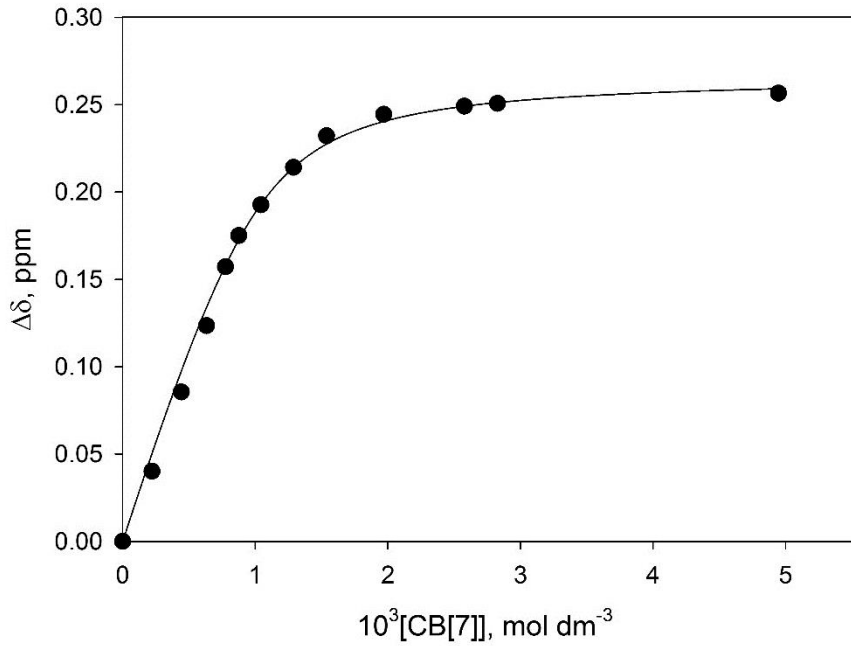


Figure S24. Plot of complexation-induced shift in the proton resonance H β for EPPS (1.03×10^{-3} mol dm $^{-3}$) as a function of [CB[7]] in D $_2$ O (pD = 4.75, 0.050 mol dm $^{-3}$ NaOAc-d $_3$ /0.025 mol dm $^{-3}$ DCl). The solid curve is a fit to a 1:1 binding model using $K_{\text{CB}[7]} = 8.86 \times 10^3 \text{ dm}^3 \text{ mol}^{-1}$ and $\Delta\delta_{\text{lim}} = 0.27 \text{ ppm}$.

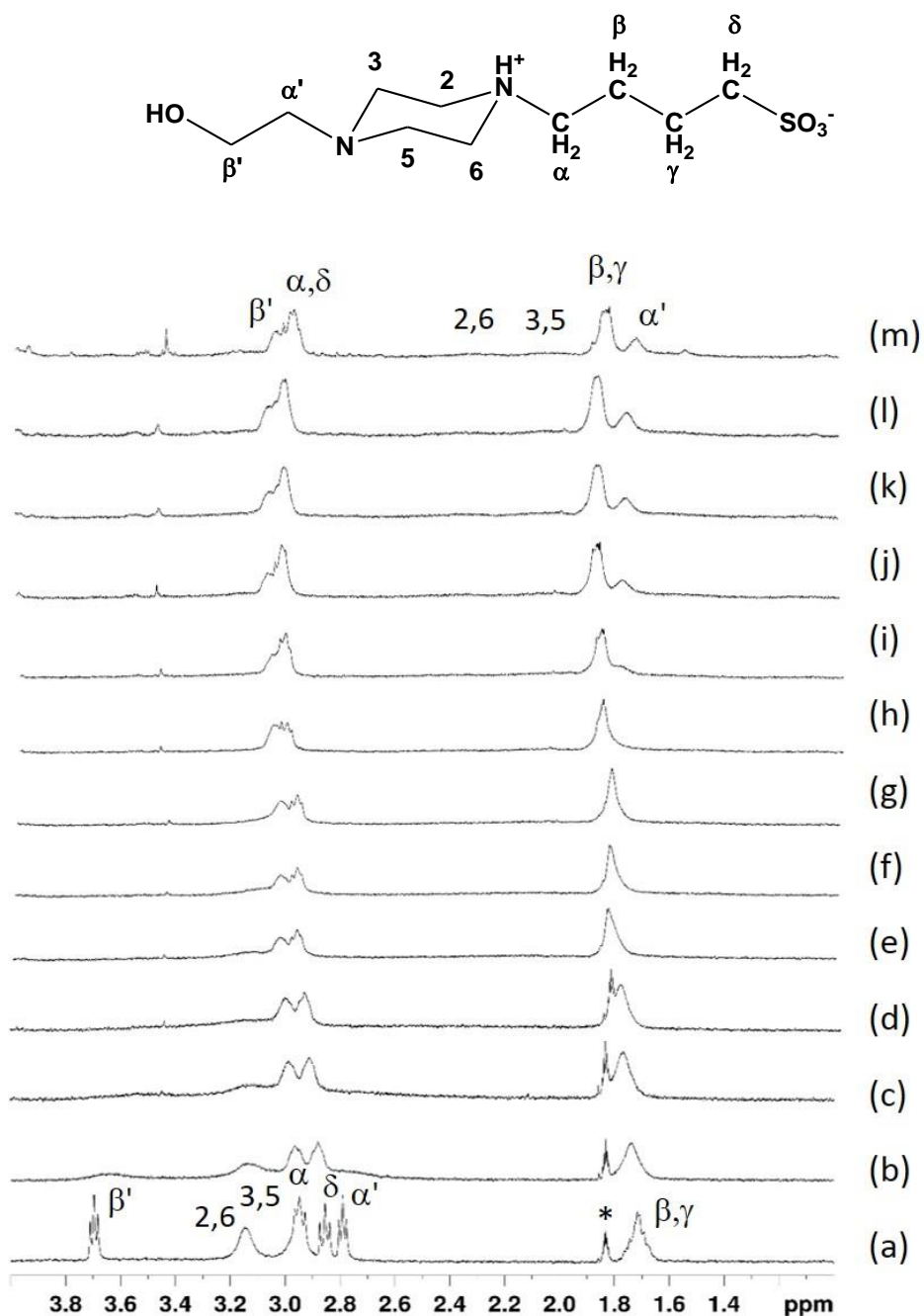


Figure S25. ^1H NMR (300 MHz) titration of HEPBS (0.976×10^{-3} mol dm $^{-3}$) with (a) 0.00, (b) 0.23, (c) 0.45, (d) 0.68, (e) 0.79, (f) 0.90, (g) 1.01, (h) 1.13, (i) 1.35, (j) 1.69, (k) 2.26, (l) 2.82 and (m) 3.39 equivalents of CB[7] in D₂O (pD = 4.75, 0.050 mol dm $^{-3}$ NaOAc-d₃(*)/0.025 mol dm $^{-3}$ DCl).

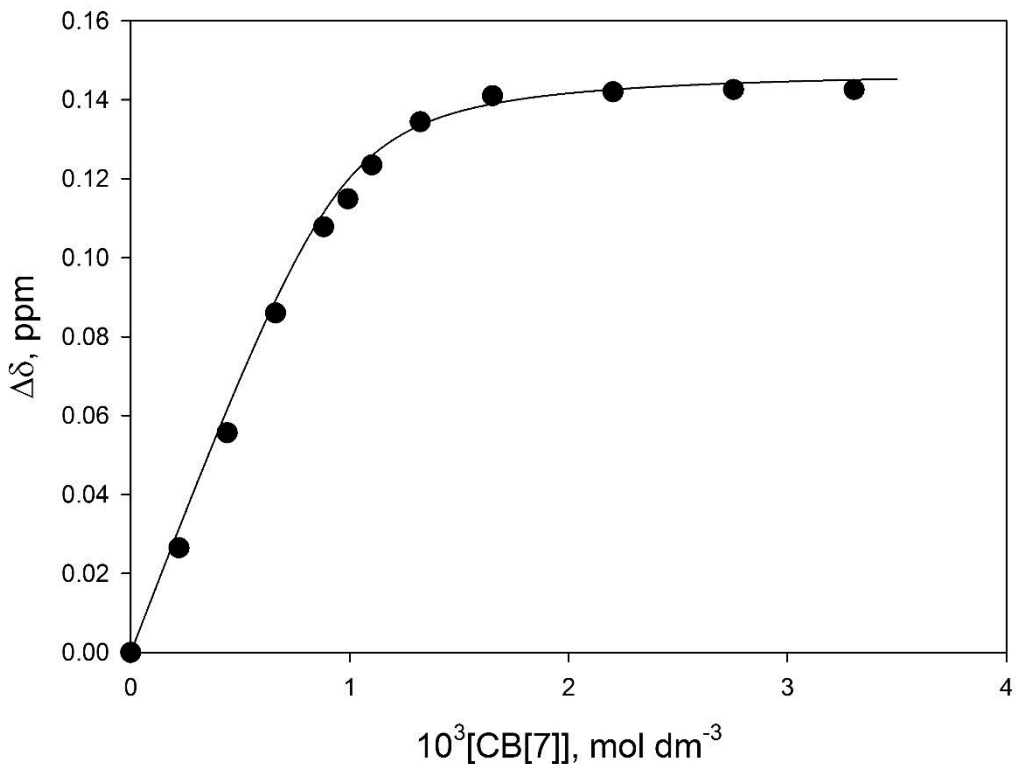


Figure S26. Plot of complexation-induced shift in the proton resonance $\Delta\delta$ for HEPBS (0.976×10^{-3} mol dm⁻³) as a function of [CB[7]] in D₂O (pD = 4.75, 0.050 mol dm⁻³ NaOAc-d₃/0.025 mol dm⁻³ DCl). The solid curve is a fit to a 1:1 binding model using $K_{\text{CB}[7]} = 2.1 \times 10^4$ dm³ mol⁻¹ and $\Delta\delta_{\text{lim}} = 0.148$ ppm.

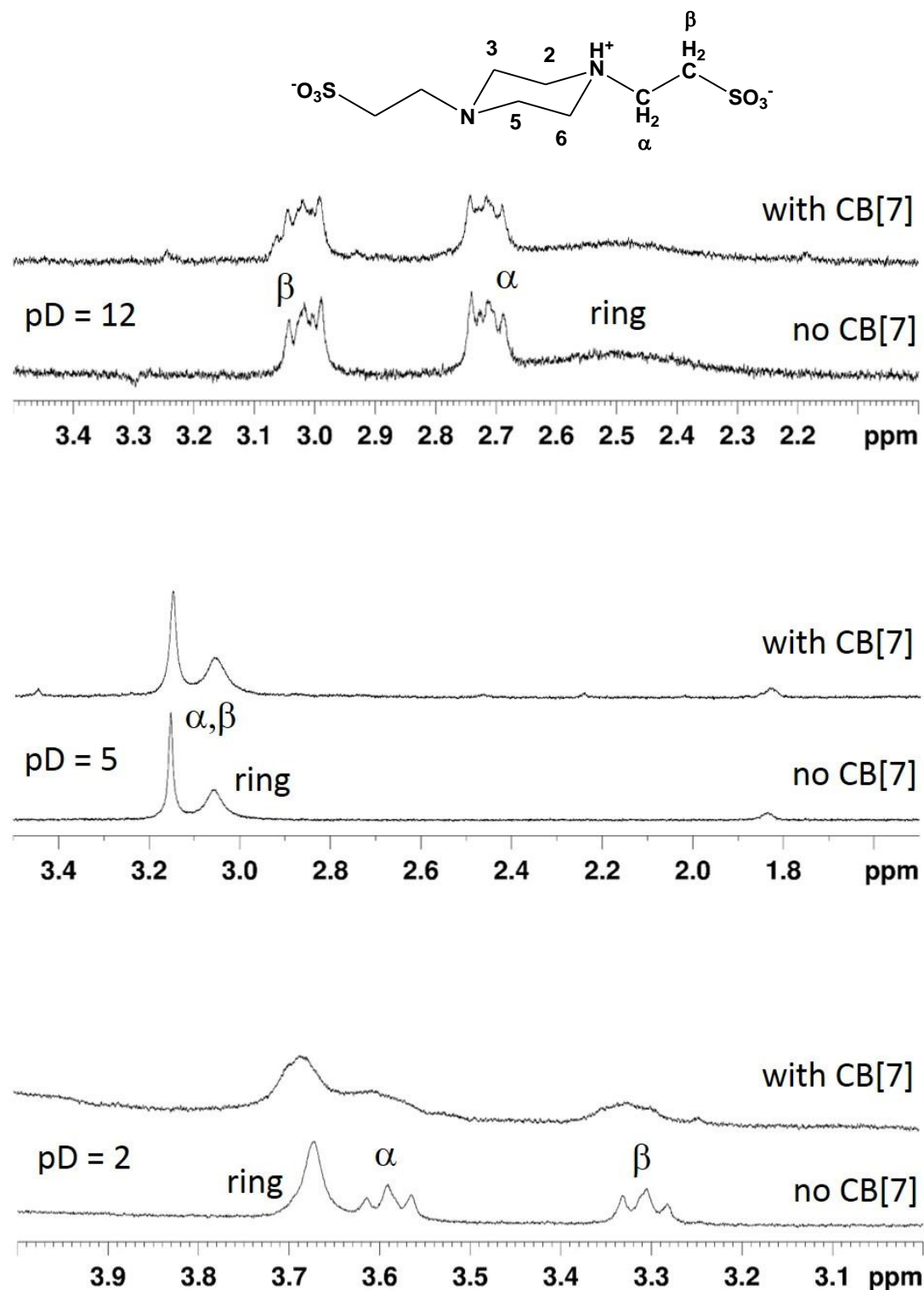


Figure S27. ^1H NMR spectra of PIPES (1.0 mmol dm^{-3}) in the absence and presence of 5.0 mmol dm^{-3} CB[7] at pD = 2 (bottom), 5 (middle), and 12 (top).

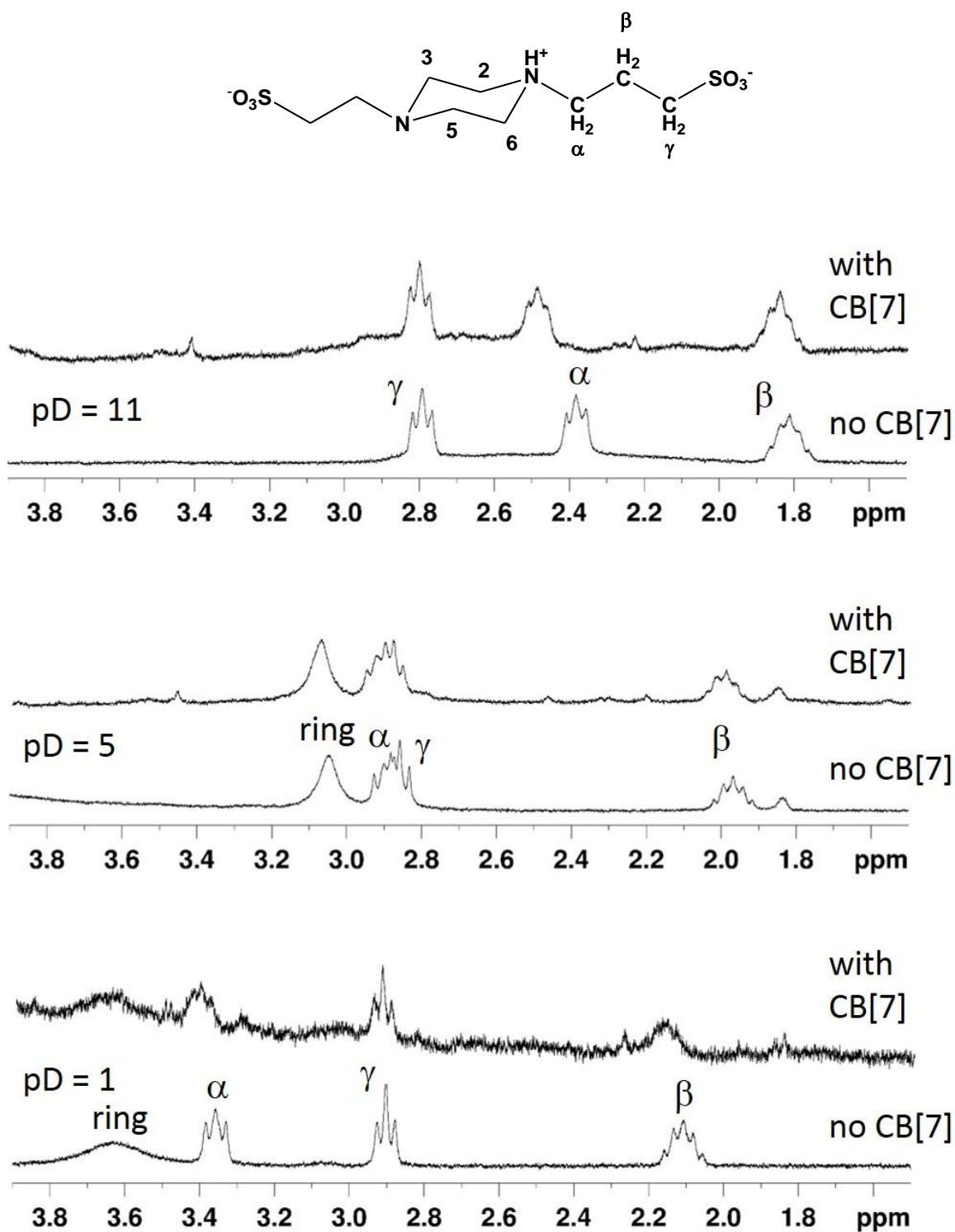


Figure S28. ^1H NMR spectra of PIPPS (1.0 mmol dm^{-3}) in the absence and presence of 5.0 mmol dm^{-3} CB[7] at pD = 1 (bottom), 5 (middle), and 11 (top).

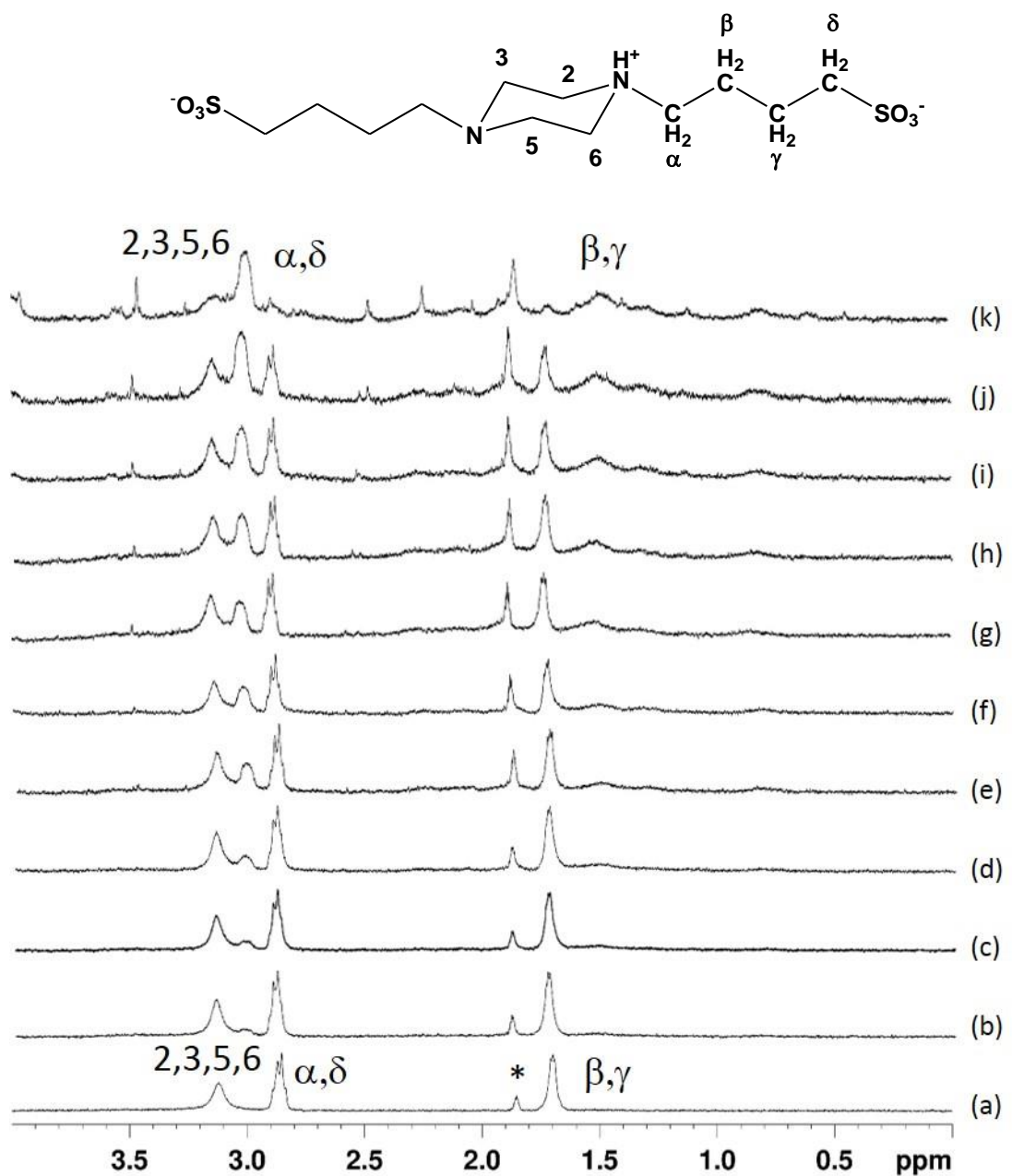


Figure S29. ^1H NMR (300 MHz) titration of PIPBS ($0.948 \times 10^{-3} \text{ mol dm}^{-3}$) with (a) 0.00, (b) 0.32, (c) 0.64, (d) 0.95, (e) 1.27, (f) 1.43, (g) 1.59, (h) 1.90, (i) 2.38, (j) 3.17, and (k) 8.15 equivalents of CB[7] in D_2O ($\text{pD} = 4.75$, $0.050 \text{ mol dm}^{-3}$ NaOAc-d_3 (*)/ $0.025 \text{ mol dm}^{-3}$ DCl).

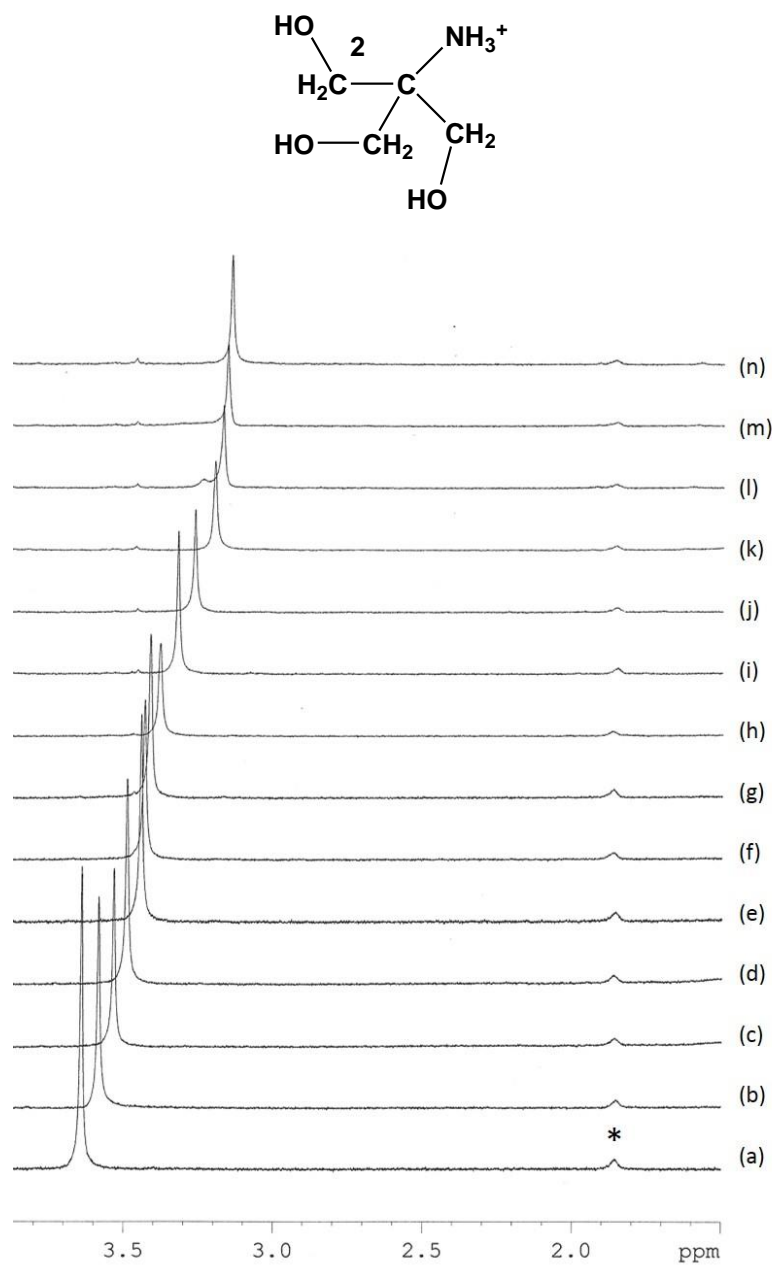


Figure S30. ^1H NMR (300 MHz) spectra for the complexation of TRIS ($1.16 \times 10^3 \text{ mol dm}^{-3}$) with (a) 0.00, (b) 0.19, (c) 0.39, (d) 0.60, (e) 0.79, (f) 0.90, (g) 0.98, (h) 1.21, (i) 1.48, (j) 1.97, (k) 2.56, (l) 2.89, (m) 3.22, and (n) 4.31 equivalents of CB[7] in D_2O ($\text{pD} = 4.75$, $0.050 \text{ mol dm}^{-3}$ NaOAc-d_3 (*)/ $0.025 \text{ mol dm}^{-3}$ DCl).

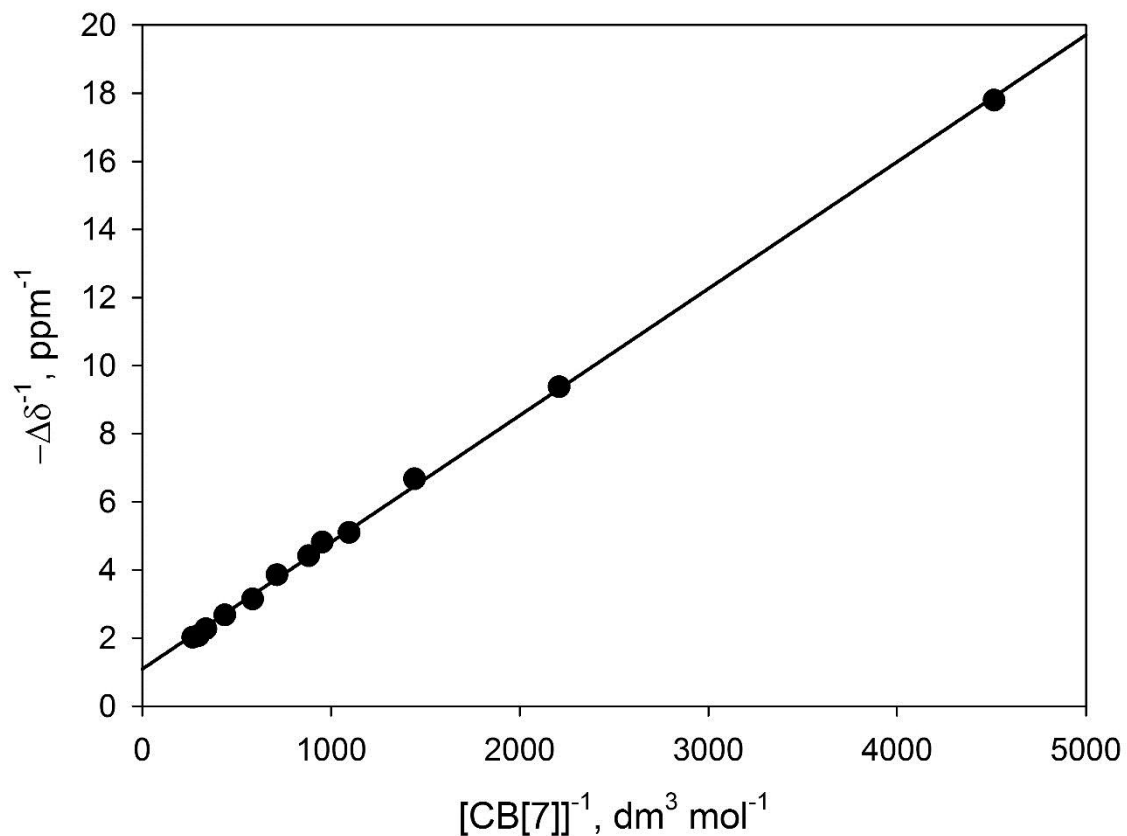


Figure S31. Double reciprocal (Benesi-Hildebrand) plot of $-\Delta\delta^{-1}$ (H_2) against $[\text{CB}[7]]^{-1}$ for the complexation of TRIS ($1.16 \times 10^3 \text{ mol dm}^{-3}$) with CB[7] in D_2O ($\text{pD} = 4.75$, $0.050 \text{ mol dm}^{-3}$ NaOAc- d_3 /0.025 mol dm⁻³ DCl). The linear regression gives $K_{\text{CB}[7]} = 291 \text{ dm}^3 \text{ mol}^{-1}$ from the intercept/slope.

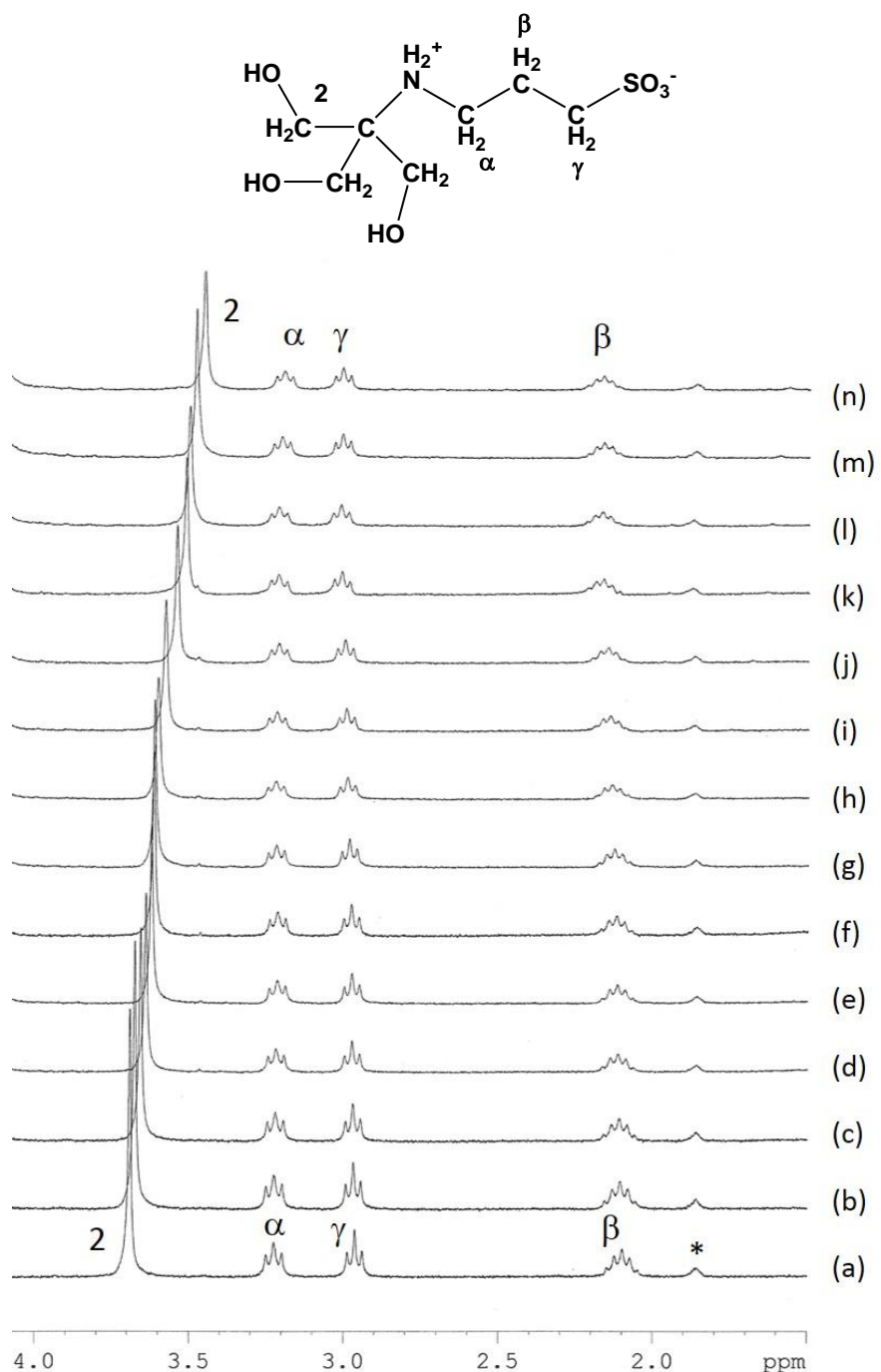


Figure S32. ^1H NMR (300 MHz) spectra for the complexation of TAPS ($0.980 \times 10^3 \text{ mol dm}^{-3}$) with (a) 0.00, (b) 0.18, (c) 0.37, (d) 0.57, (e) 0.75, (f) 0.86, (g) 0.90, (h) 1.12, (i) 1.45, (j) 1.87, (k) 2.27, (l) 2.73, (m) 3.31, and (n) 5.23 equivalents of CB[7] in D_2O ($\text{pD} = 4.75$, $0.050 \text{ mol dm}^{-3}$ NaOAc-d_3 (*))/ $0.025 \text{ mol dm}^{-3}$ DCl).

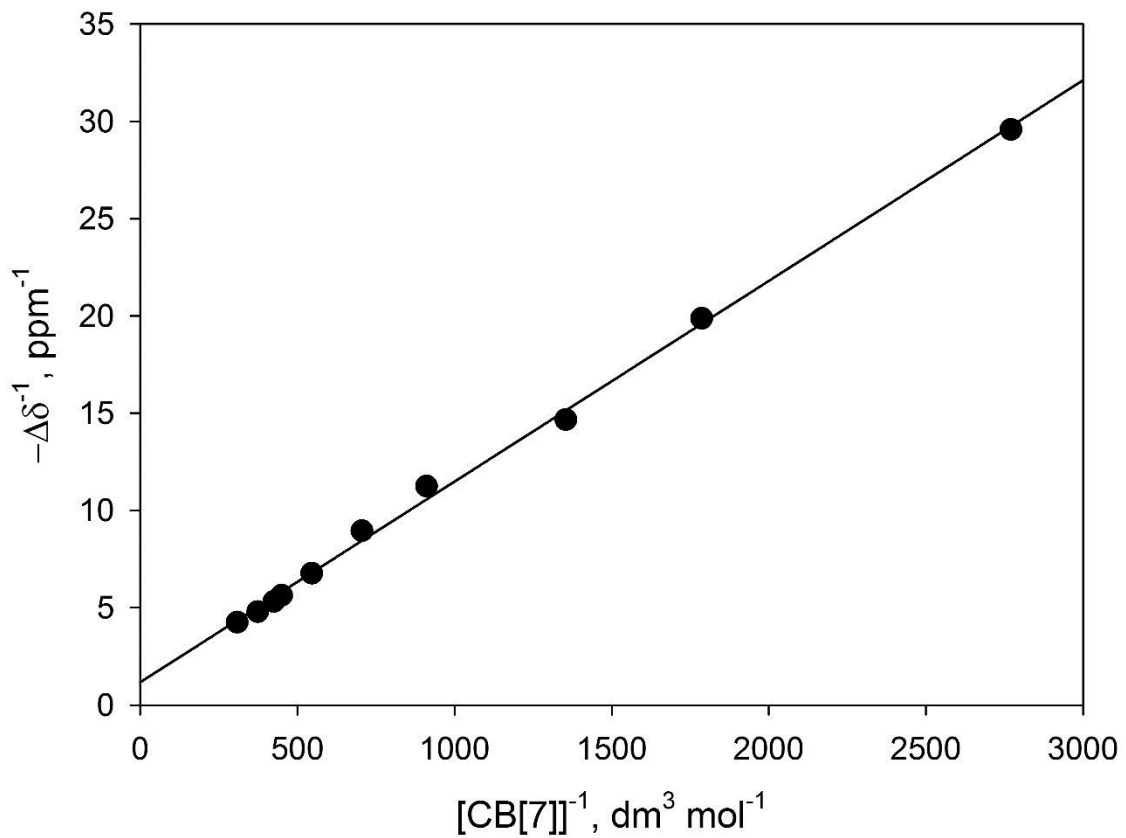


Figure S33. Double reciprocal (Benesi-Hildebrand) plot of $-\Delta\delta^{-1}$ (H_2) against $[CB[7]]^{-1}$ for the complexation of TAPS (0.980×10^3 mol dm⁻³) with CB[7] in D₂O (pD = 4.75, 0.050 mol dm⁻³ NaOAc-d₃/0.025 mol dm⁻³ DCl). The linear regression gives $K_{CB[7]} = 113$ dm³ mol⁻¹ from the intercept/slope.